2008

Fabrication of Nanostructured Metals and Their Hydrogen Storage Properties

Asli Ertan
Cleveland State University

FABRICATION OF NANOSTRUCTURED METALS AND THEIR HYDROGEN STORAGE PROPERTIES

ASLI ERTAN

Bachelor of Science in Chemical Engineering

Ege University

June 1999

Master of Science in Chemical Engineering

Izmir Institute of Technology

February 2004

submitted in partial fulfillment of requirements for the degree

DOCTOR OF ENGINEERING IN CHEMICAL ENGINEERING

at the

CLEVELAND STATE UNIVERSITY

October 2008

This dissertation has been approved for the Department of Chemical and Biomedical Engineering and the College of Graduate Studies by

---

Dr. Orhan Talu, PhD
Department of Chemical Engineering
Cleveland State University

Date

Dr. Surendra N. Tewari, PhD
Department of Chemical Engineering
Cleveland State University

Date

Dr. D.B. Shah, PhD
Department of Chemical Engineering
Cleveland State University

Date

Dr. Nolan Holland, PhD
Department of Chemical Engineering
Cleveland State University

Date

Dr. Petru Fodor, PhD
Physics Department
Cleveland State University

Date

DEDICATION

This thesis is dedicated to

Umit Ertan, my dearest dad…

ACKNOWLEDGMENTS

I would like to thank department of energy (DOE) for their financial support to this study (contract# DE-FC 36-04ER14007**).**

I would like to express my intimate gratitude to my academic advisor, Dr. Orhan Talu, for his guidance, support, encouragement and his advices on my career development and personal life. It has been my great fortune and honor to earn my degree under his supervision. I would like to thank my co-advisor, Dr. Surendra N. Tewari, for his great help and valuable suggestions through the course of my research. I would like to thank my dissertation committee members Dr. D.B. Shah, Dr. Nolan Holland and Dr. Petru Fodor for being on my committee and for their contributions to my thesis study.

I would like to thank Jim Barker, Ali Kaddah, David Epperly for their technical support to my research.

I would like to give my special thanks to Ms. Becky Laird and Ms. Darlene Montgomery for their helps and friendship during my study.

I finally would like to express my deep appreciation to my dearest parents Nurdal and Umit Ertan, my sister Pelin Ertan for always being there for me, for their peerless support and guidance all throughout my life. I would especially like to thank my husband as well as my colleague Ozge Can for accompanying me in this journey, giving me the strength to face the challenges. I am grateful for his endless love, support and patience.

FABRICATION OF NANOSTRUCTURED METALS AND THEIR HYDROGEN STORAGE PROPERTIES

ASLI ERTAN

ABSTRACT

Searching for new energy sources is highly desirable for the next generations when rapidly changing factors are considered such as population, increasing pollution and exhaustion of fossil fuels. Hence, there is a need for clean, safe and efficient energy carriers or forms of energy that can be transported to the end user. One of these energy carriers is electricity which has been used widely and can be produced from various sources. However, its production from fossil fuels contributes to pollution. On the other hand hydrogen, due to its abundance, light weight, low mass density, high energy density and non-polluting nature attract many researchers' attention to be used as an energy carrier so that the dependence on fossil fuels would be minimized which are responsible for global warming due to harmful emissions to the atmosphere. In addition, hydrogen can be converted to other forms of energy more efficiently through catalytic combustion, electrochemical conversion, etc. However, hydrogen must be handled extremely carefully due to its physico-chemical properties. Its on-board storage is a major challenge because

of its high explosiveness and the high cost of the storage process. There are many factors that need to be considered when deciding upon the storage method and the most important ones are safety, gravimetric and volumetric capacities, cost, environmental friendliness, reversibility and release rate.

This work is dedicated to study the hydrogen uptake behavior of nanostructured palladium constructed through template-assisted electrochemical deposition process. Hydrogen sorption experiments were conducted using a custom-made volumetric system. Nickel was used as the test metal to tune the electrochemical deposition process before conducting the experiments with palladium. Growth mechanism of the nanostructured metals in various substrates was investigated. Conditions for growing nano-scaled palladium were optimized and the hydrogen sorption experiments were conducted at various temperatures. The pressure-composition (P-C) isotherms revealed the nanostructuring effect on the hydrogen uptake behavior of palladium nanowires with 100-200 nm pore diameters.

TABLE OF CONTENTS

LIST OF TABLES

LIST OF FIGURES

LIST OF ABBREVIATIONS

SEM	Scanning electron microscopy
EDX	Energy dispersive X-ray spectrometry
P-C	Pressure-composition isotherm
OCP	Open circuit potential
WE	Working electrode
CE	Counter electrode
FC	Flow controller

CHAPTER I

INTRODUCTION

It has become crucial to develop an alternative energy source due to global warming and rapid depletion of the available oil reserves in the near future. Hence, there is a need for clean, safe and efficient energy carriers or forms of energy that can be transported to the end user. One of these energy carriers is electricity which has been used widely and can be produced from various sources. However, its production from fossil fuels contributes to pollution. Hydrogen on the other hand is considered to be the ideal energy carrier due to its superior properties such as abundance, light weight, environmental friendliness and easy synthesis. Also, it can be converted to other forms of energy more efficiently than any other fuel through catalytic combustion, electrochemical conversion, etc. The storage of hydrogen in an economical and safe way is the major challenge in developing the hydrogen economy. The conventional methods such as high pressure gas, cryogenic liquid suffer from different limitations such as safety, efficiency or high cost [1-9]. Therefore, sufficient storage of hydrogen in a safe and economical way

while meeting all consumer necessities is a major issue to be solved to improve hydrogen power systems.

Metal hydrides have the clear advantages over conventional methods because of their high gravimetric and volumetric densities, safe operating conditions, easy formation, etc. However, one disadvantage with these systems is their slow kinetics. Nanotechnology helps to improve the kinetic behavior of metal hydrides. Nanostructured materials which make up the metal hydrides significantly improve the reaction rates due to their large surface area. They provide dilated lattices which result in larger interstitial volumes for hydrogen storage. It has been well known that along the grain boundaries of nanocrystalline materials, hydrogen diffusion is much faster which improves the kinetics for hydrogen adsorption and desorption when compared to their bulk counterpart. Hydrogen ion diffusion length is reduced with nanoparticles due to smaller particle size which results in faster dynamics for hydrogen sorption. Another issue is the reversibility. Nanocrystalline materials have open and flexible structures that are resistant to decrepitation due to morphological changes during hydrogen adsorption/desorption processes. Due to these reasons, recently, the possibility of storing larger amounts of hydrogen on high surface area of nanomaterials attracted great interest leading to detailed investigation of hydrogen sorption capacities of these materials [10]. The ultimate goal of these studies is determined by the immediate need of storing hydrogen in the most efficient way so that it can be commercialized and hence reduce our dependence on fossil fuels. One of the main purposes of our research is to produce nanostructured materials and understand the hydrogen uptake behavior of these unique materials. We believe that investigating the fundamental hydrogen sorption properties of nanostructured metal-

hydride systems opens the doors for using this system as the future hydrogen storage method.

In this study, palladium hydride was selected as the model system to determine the nanostructuring effect since its bulk properties are well-known. Nickel was used as the test metal before fabricating the palladium nanowires due to their high cost. Electrochemical deposition was used to produce the nanostructured materials. A better control over the dimensions of the fabricated materials can be exercised by electrochemical deposition process. After obtaining the nanostructured materials, hydrogen sorption properties of these materials were investigated by a lab-made volumetric uptake system. The examination of the hydrogen uptake of the nanostructured materials which have been produced by electrochemical deposition is unique since the hydrogen sorption studies performed to date are usually applied to the nanostructured materials obtained by ball-milling. However, it is well known that the nano-scaled materials produced through high energy ball-milling aggregate to reduce their surface energy. In addition, imprecise milling charge may lead to erratic variations in the measurements which is not desired [11-12].

1.1 Specific aims of the study

Hydrogen sorption properties of palladium hydride system were examined with nanostructured palladium fabricated through template-assisted electrochemical deposition using a custom-built volumetric system. In order to achieve our goal, we have practiced the below stated tasks.

1. Conducting electrodeposition experiments to tune electrodeposition process by using nickel as the test material.
2. Fabricating palladium nanowires using a single-step electrochemical deposition method without using any additives to prevent the addition of different growth parameters to the system.
3. Modifying a custom-built volumetric system to conduct hydrogen sorption experiments.
4. Constructing palladium-hydride system phase diagram by conducting equilibrium hydrogen sorption experiments.
5. Determining the hydrogen uptake properties of these materials and investigating the nanostructuring effect.

1.2 Thesis organization

In chapter II, a detailed background about hydrogen technology is presented. Different hydrogen storage methods are described but more emphasis is given to metal hydride systems since the proposed research is based on the superior properties of metal hydrides. Afterwards, information on nanotechnology is provided and the advantages of producing nanostructured metal hydride systems are described.

Afterwards, methodology of how to construct metal hydrides and the methods to conduct hydrogen sorption experiments are given in chapter III, in the experimental section. Chapter IV presents the results and discussion of both electrodeposition and hydrogen sorption studies. Finally, in Chapter V, conclusions of the study are presented.

CHAPTER II

BACKGROUND

2.1 Hydrogen Technology

Searching for new energy sources is highly desirable for the next generations when rapidly changing factors are considered such as population, increasing pollution and exhaustion of fossil fuels. Hence, there is a need for clean, safe and efficient energy carriers or forms of energy that can be transported to the end user. Hydrogen with its unique properties such as abundance, light weight, low mass density, high energy density and non-polluting nature attract many researchers' attention as an ideal carrier and minimize the use of fossil fuels which are responsible for global warming due to carbon dioxide emissions to the atmosphere. The possible consequences of global warming threaten the safety of many organisms in mild climate countries and cause various natural disasters such as hurricanes, floods, ice storms, forest fires, etc. [1-9] .

Another promising factor for the employment of hydrogen as the alternative energy carrier is its easy synthesis from various renewable sources such as biomass, hydro, wind, geothermal and solar energy as well as fossil fuels and nuclear energy without the emission

of pollutants or greenhouse gases [2,4,6,9,13]. Hydrogen can also be converted to other forms of energy more efficiently than any other fuel through different processes such as catalytic conversion, electrochemical conversion and hydriding [14].

However, hydrogen must be handled extremely carefully due to its physico-chemical properties. Its on-board storage is a major challenge because of its high explosiveness and the high cost of the storage process. Therefore, hydrogen storage has been the subject of extensive research for many years. It is one of the key technologies particularly for the development of both mobile and stationary applications and to have cleaner, more efficient and less costly energy systems [2,5,9,13-14]. Thus, advancement of hydrogen storage is crucial to make hydrogen an important element of the world's energy economy.

Hydrogen can be stored in several different ways such as pressurized gas, cryogenic liquid, in the form of chemical compounds, etc [3,4-5]. There are many factors that need to be considered when deciding upon the storage method and the most important ones are safety, gravimetric and volumetric capacities, cost, environmental friendliness, reversibility and release rate [5,8,13,15-16].

The traditional methods available have one or more of these limitations. For example, high pressure compressed gas tanks suffer from safety, high cost of the storage process and not fulfilling the capacity target of hydrogen storage for the future. Major drawback with this method is its limitation in terms of size and shape. More effort and time needs to be spent to optimize all of these factors.

Liquid hydrogen tanks normally can store hydrogen more than high pressure gas tanks since the volumetric capacity of liquid hydrogen is more than that of the pressurized gas. However, storing hydrogen in cryogenic liquid form requires a refrigeration unit which

increases the weight and energy cost. Another key issue with this method is that hydrogen boils-off which in turn results in as much as 40% loss in energy content. Other than cost and energy, boiling-off hydrogen creates problems in terms of refueling frequency and safety especially for vehicles parked in closed places [2,5].

One other means to store hydrogen is using carbon adsorbents. Normally, gas adsorption on solid materials is safe and the large surface area of these porous materials could be utilized for hydrogen storage purposes. However, activated carbons are not effective in storing hydrogen because these materials have narrow pore size distribution and hence, only a small section of the pores are small enough to interact strongly with the hydrogen molecules at moderate temperatures and pressures. Therefore, good storage capacity can be achieved only at cryogenic temperatures. Because of these reasons, activated carbons are also not very efficient to store hydrogen [5].

Chemical hydrogen storage is another option that has the advantage of offering high energy densities. One of the examples of these chemical storage options is the hydrolysis reactions that engage the chemical reaction of hydrides with water to produce hydrogen. However, most of these reactions are irreversible meaning that the material used to store hydrogen needs to be regenerated off-board the vehicle which makes it quite impractical. [2,10,13].

One other option to store hydrogen is metal hydride systems where the hydrogen can be stored as solid-state at moderate temperatures and pressures. The proposed research is based on metal hydrides, therefore, this class of storage is explained in further detail in the following section.

2.1.1. Metal Hydrides

Hydrogen forms metal hydrides; a class of solids formed when certain metals are exposed to hydrogen gas. Metal-hydride systems involve solid-state storage of hydrogen at moderate temperature and pressure which give them the advantage of operating at safe conditions [2]. Metal hydrides are composed of metal atoms which make-up the host lattice for the hydrogen atoms. In general, when hydrogen molecule interacts with the metal surface, it splits into hydrogen atoms and then enters the metallic lattice. The atoms diffuse through the metal and move in between the interstitial sites of the metal lattice which is the hydride phase [3, 6].

Hydriding mechanism can be investigated in more detail at a molecular scale. The interaction of the hydrogen molecule with the metal surface corresponds to the minima in the potential curve which indicates that molecular adsorption, atomic adsorption and bulk absorption are taking place in the system [1]. Physisorption of the hydrogen molecule on the metal surface is the first step which means that the molecule sticks on the surface physically usually by either Van der Waals or electrostatic attraction without forming any chemical bonds. Physisorption is a reversible process which depends on the temperature and pressure. If the temperature and the pressure are high enough, the physisorbed hydrogen is dissociated into its atoms and becomes chemisorbed. Chemisorption is defined as the combination of hydrogen with the metal to form a new compound and both parties change chemically as a result of this process. During this process, electron transfer between the hydrogen and the metal takes place and this may involve the thermal or catalytic activation due to the dissociation energy barrier. Hydrogen atoms “penetrate” the surface during chemisorption. After that, the hydrogen atoms diffuse to the metal sublayers and hydride formation at the metal/hydride interface takes place (Figure 1) [17].

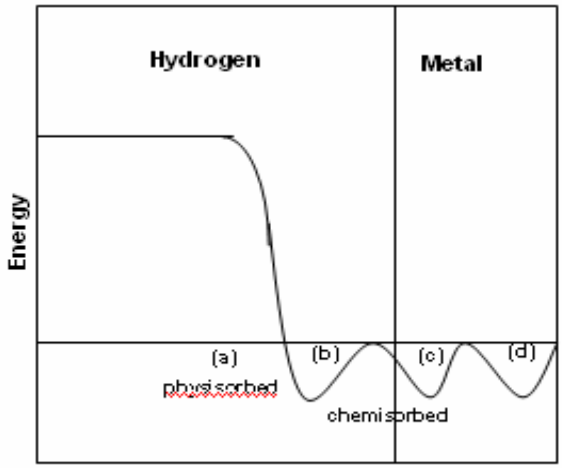

Figure 1. Potential energy curve for the Lennard Jones potential exhibiting hydrogen binding to the metal: (a) physisorption (b) dissociation (c) chemisorption on sublayer sites (c) and (d) diffusion [1]

An ideal solid for hydrogen storage would be a structure having nanopores to increase the surface area. Having high hydrogen storage capacity per unit mass and unit volume, low dissociation temperature, moderate dissociation pressure, low heat of formation necessary to reduce the energy when releasing hydrogen, reversibility constitute some of the most important reasons for metal hydrides being so popular recently for hydrogen storage applications [1-3,9].

Sorption of hydrogen by the metal structure is an exothermic process. When metal hydrides absorb hydrogen heat is released. In contrast, heat is required to release hydrogen atoms from the metal lattice. The schematic diagram of the process is shown in Figure 2. The upper part of the diagram shows the absorption process where hydrogen

molecules are attached to the metal surface and break down to hydrogen atoms. Metal hydrides are formed when the hydrogen atoms penetrate into the metal structure. The lower part of the diagram shows the desorption process where hydrogen atoms leave the metal structure and combine to form hydrogen molecules.

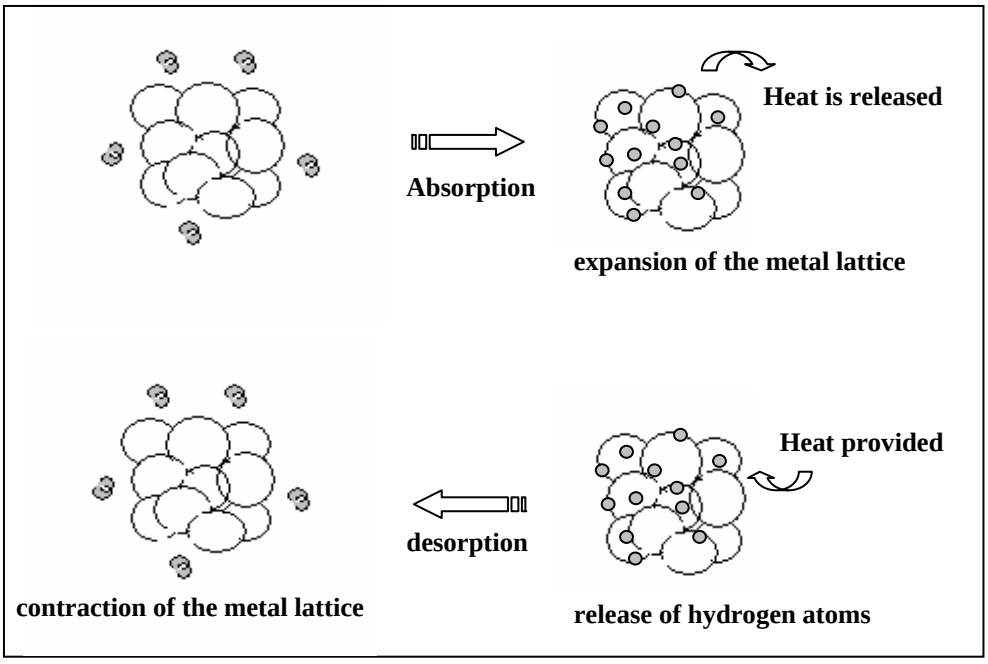

Figure2. Hydrogen sorption process

The changes in pressure and concentration of the metal-hydride system at constant temperature and closed system can be followed experimentally. The results of the experimental measurements can be used to construct the pressure-composition (P-C) isotherm of metal-hydride systems that relate the equilibrium pressure of hydrogen to the hydrogen content of the metal (Figure 3) [18-19].

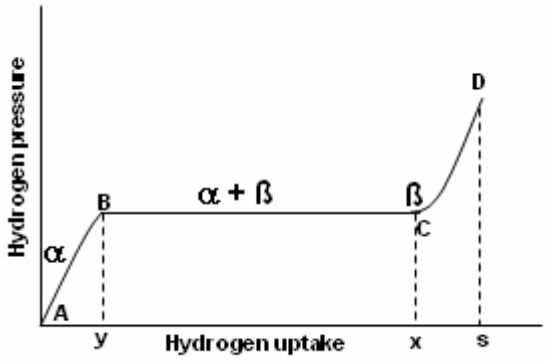

Figure 3. Representative pressure-composition (P-C) sorption isotherm [19]

The P-C isotherm of metal-hydride systems has three distinct parts. The initial steep step of the isotherm from A to B represents the hydrogen dissolving in the metal to form the solid solution phase. It is also called the α phase. At point B, saturation limit of solution phase is reached, hydride phase begins to appear and a second phase begins to form which is called as the ß phase. From point B to C, pressure remains constant in most metal hydrides while concentration of hydrogen increases with the rapid conversion of α into ß phase. The process of conversion is completed at point C where only ß phase remains which is the metal hydride. When the transition is completed, system regains a degree of freedom which results in an increase of pressure with the further addition of hydrogen. The constant segment of this isotherm indicates the pressure of hydrogen in equilibrium with the metal-metal hydride (α+ß) phases. This pressure is also called the dissociation pressure of the metal hydride at the specific temperature, or the plateau pressure [18-19].

Hysteresis effects can be observed in most of the metal-hydride systems for the α to ß conversion and the reverse ß to α process. Hysteresis is indicated by the absorption

and desorption branches not following each other. Usually, the absorption plateau is higher than desorption plateau. The reaction of hydrogen with a metal can be expressed as a reversible reaction:

$$M + \frac{x}{2} H_2 \Leftrightarrow MH_x \qquad [1]$$

Recently, metal hydrides have been the focus of intensive research for hydrogen storage purposes because of the superior properties stated in this section. Metal hydrides are the promising candidates for the future due to their high volumetric hydrogen storage capacity and safety advantage. Thus, recently, rigorous research has been conducted on metal hydrides to improve their hydrogen adsorption/desorption properties such as kinetics, toxicity, thermal properties, hydrogen storage capacity, etc. [2].

2.1.1.1 Palladium Hydride

The bulk properties and several physical parameters of hydrogen-palladium system have been extensively studied for many years dating back to the 19th century and is considered as the classic metal-hydride system in literature [10, 20-22]. The reason for this is mainly due to the availability of the pure bulk samples so that no surface treatments are needed. This study concentrates on the effect of nanostructuring, thus the well-known bulk palladium hydride system properties is an advantage.

Palladium is in the second transition metal series with 10 electrons in the 4d electron shell. It has high hydrogen sorption capacity at room temperature. Palladium has a face centered cubic (fcc) structure [10]. Many computational studies have been made on

different planes of palladium surfaces to better understand the palladium-hydride systems. Among all the surfaces palladium have, most of the studies have been focused on (1 1 1) plane which has the highest packing density (Figure 4).

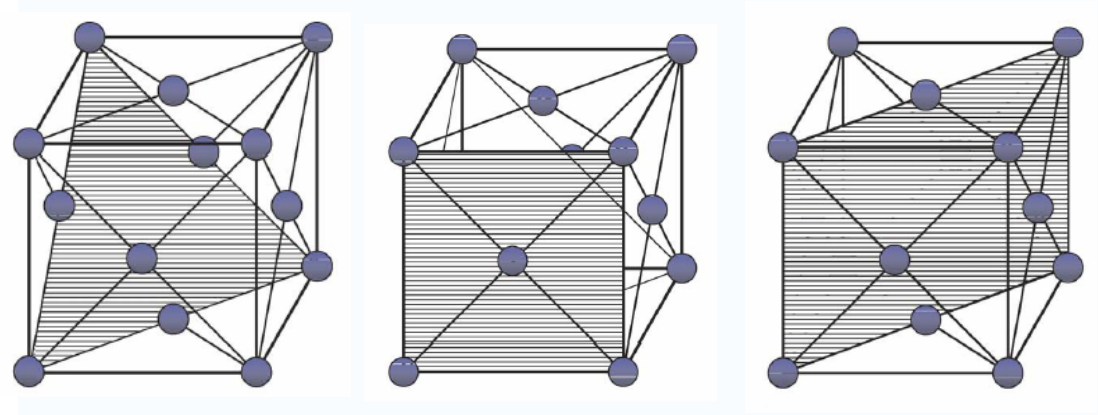

(a) **(b)** **(c)**

Figure 4. Palladium unit cell showing (a) (1 1 1) (b) (1 0 0) and (c) (1 1 0) planes [20]

There are four different adsorption sites for hydrogen atoms located on the (1 1 1) plane: A bridge site between two palladium atoms, on top of a palladium atom, in a hollow between three palladium atoms and finally in fcc site in a hole in the layer directly beneath the surface layer. As a result of computational studies, it was shown that fcc is the most stable site for the hydrogen molecules. There are three possible sites for adsorption for (1 0 0) plane: a hollow between four palladium atoms, a bridge between two surface atoms and finally, on top of a palladium atom. Among these, it was shown that hollow site is the most favorable one for hydrogen atoms. For the hydrogen

adsorption on (1 1 0) plane the favorable sites could not be obtained clearly since the requirements for the computational studies are highly complicated [20].

As hydrogen dissolves in palladium metal the hydrogen atoms occupy the octahedral interstitial sites of the fcc metal sublattice. This process results in moving apart the nearest neighbor atoms further so that more room becomes available for the hydrogen atoms entering the metal lattice (Figure 5).

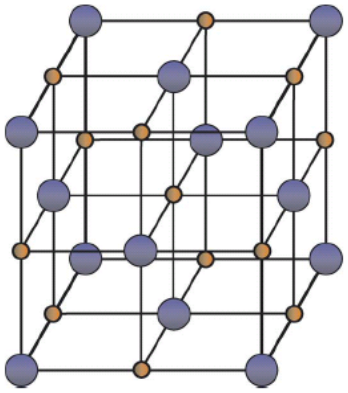

Figure 5. Unit cell of palladium metal showing octahedral sites that would be occupied by hydrogen, large spheres are palladium and small spheres are hydrogen [20]

It is well known that hydrogen rapidly dissociates on palladium surfaces and when the hydrogen gas splits into atoms on the palladium surface, they diffuse through the sublayers of the metal and form the palladium-hydride. Equilibrium is attained between the gas phase hydrogen molecules and the adsorbed surface atoms [22-25]. The lattice constants of the system vary depending on if the hydride is in α or β phase. The α phase is the solution phase and at this stage, the lattice constants are close to palladium

metal. The H to Pd ratio for this phase is 0.03. As more hydrogen is introduced to the system, more hydrogen dissolves which results in an increase in the lattice constants with pressure. It was found that for pure palladium the lattice of α-PdH_x increases slightly from 3.889 Å to 3.893 Å due to hydrogen sorption. The composition in the β phase is around 0.6 at room temperature. At this stage where the structure is fcc, the lattice constant increases up to 4.04 Å [20].

2.2 Nanotechnology

One disadvantage with metal hydride systems is the slow dynamics of hydrogen uptake and release [6]. This limitation can be overcome by producing large surface area materials which in turn increases the overall hydrogen dissociation reaction rate and decreases the diffusion time constants. Therefore, physical and chemical properties of metal hydrides can be tailored drastically by reducing the size of metal hydride particles in nanometer scales [1, 8].

Nanotechnology is a general term for various technologies focusing on designing, modifying and controlling the physical and chemical properties of materials. Nanoscaled metals with large surface area and porosity are expected to be excellent materials for hydrogen storage [21]. One of the reasons for that is they provide dilated lattices which result in larger interstitial volumes for hydrogen storage. It has been well known that along the grain boundaries of nanocrystalline materials hydrogen diffusion is much faster which improves the kinetics for hydrogen adsorption and desorption when compared to their bulk counterpart. Also, with nanoparticles hydrogen ion diffusion length is reduced due to smaller particle size which results in faster hydrogen sorption. One last issue is the reversibility. Nanocrystalline materials have open and flexible structures that are resistant

to decrepitation due to morphological changes during hydrogen adsorption/desorption processes [1,10]. Due to these reasons, recently, the possibility of storing larger amounts of hydrogen on high surface area of nanomaterials attracted great interest leading to detailed investigation of hydrogen sorption capacities of these materials [26].

2.2.1. Methods to make nano-scaled metals

Nanostructured materials can be formed in various ways. Laser ablation, vapor condensation, sputtering, ball milling of the metal are some of the techniques to produce nanostructured materials. Among these, ball milling is one of the most commonly used methods due to its scalability and convenience. In this process, metal is placed in a rotating cylinder with grinding media such as ceramic balls. Due to high energy collisions between the metal and the grinding media, smaller particles are formed. The particle size range of the resulting material is around 10-50 nm which aggregate into larger particles, 300-2000 nm. The major disadvantage with ball-milling is that it is not efficient due to high energy cost of the process [1,27]. Ball-milling generally results in irregular, non-structured materials. Another important drawback with ball milling process is that small particles aggregate over time to reduce their surface energy and this is not a desired situation to study hydrogen uptake since agglomerated particles may obscure the nanostructuring effect [1].

Another form of nanostructured materials is metal nanowires, nanotubes, nanobelts which consist of an important aspect of effort in nanotechnology. Due to long range regularity of the structure, these unique materials have numerous potential applications other than hydrogen storage such as optical and magnetic media, sensors,

electronic devices, catalysis, etc. [28-35]. Many techniques have been developed to produce these nanostructured metal materials such as electrochemical deposition, electroless deposition, chemical vapor deposition, electron beam lithiography, etc. [35]. Among these, template assisted electrochemical deposition also known as electrodeposition is the most commonly used because it is an inexpensive yet elegant approach for the fabrication of the free-standing nanowires or nanorods or nanotubes [30,34]. Furthermore, it does not require the employment of complex instrumentation and one can obtain high growth rates. Crystal morphology as well as the size and shape of the material can be controlled easily and accurately. One other advantage is that extremely high aspect ratios approaching thousands can be obtained with this technique [36-39]. The structure of metal formed by electrochemical deposition from a solution containing metal ion can be controlled by the nature of the template used, electrodeposition conditions and electrolyte concentration [40].

2.2.2 Electrodeposition in porous materials

In template electrodeposition, metal is electrochemically reduced in natural or artificial pores of a membrane on a conducting substrate and then the template is removed [39]. The nanofibers are grown in the pores of the membrane systematically. In the first stage metal is electrodeposited into the pores of the membrane until they are filled up to the top surface of the membrane. Secondly, metal grows out the pores and forms hemispherical caps on the membrane surface which result in a large increase in current. Finally, caps coalescence into a continuous film as a result of the overgrowth. The corresponding schematic diagram showing nanowire growth is presented in Figure 6.

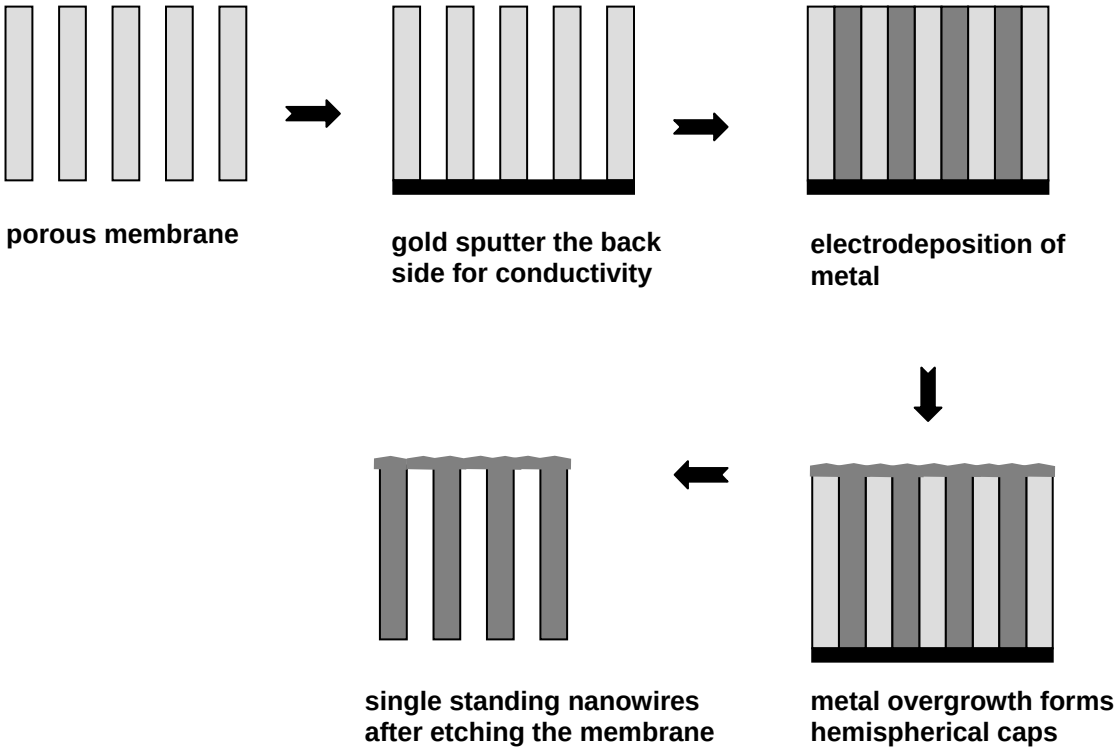

Figure 6. Schematic diagram showing nanowire growth

Electrochemical deposition experiments can be conducted both galvanostatically and potentiostatically. In potentiostatic experiments, a constant potential is applied, changes in the current with time are followed. In contrast, with galvanostatic experiments, current is kept constant while the changes in potential with time are followed. Figure 7 shows a characteristic deposition curve where the experiments are conducted at a constant potential. There is a sharp decrease in current as soon as a potential difference is applied to the system due to charging of electric double layer. The sharp decrease is due to the formation of ion diffusion barrier. Then, the current remains constant where the pores are being filled up. The following sharp increase in current is an indication of the overgrowth on the surface of the template.

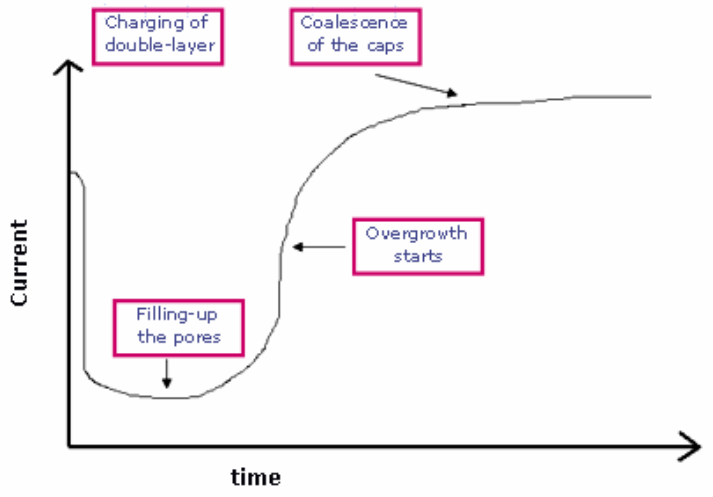

Figure 7. Characteristic deposition curve for potentiostatic experiments

2.2.3 Various templates as porous materials

Various templates have been used during template electrodeposition. The most common ones are anodized alumina and track-etch polycarbonate membranes. Other membranes used to grow nanostructured materials are: nanochannel array on glass, radiation track-etched mica, mesoporous materials, porous silicon from electrochemical etching of silicon wafer, carbon nanotubes, zeolites, etc. [27].

In this study, commercial as well as lab-made anodized alumina membranes and track-etched polycarbonate membranes were used to fabricate nanostructured materials. The lab-made alumina templates were produced by anodization process using solutions of sulfuric, oxalic and phosphoric acids and have hexagonal pore arrangement. It is well known that changing the anodizing conditions can control the structural parameters of alumina [41]. Through anodization process alumina with superior characteristics including uniform pore dimensions, good mechanical strength, thermal stability and large

surface area can be obtained [42]. One disadvantage with alumina templates is their handling. Complete removal after nanowire growth is a tedious procedure with wet-chemical etching.

Track-etched polycarbonate membranes have a uniform and controlled pore structure which can produce homogenenous, continuous and uniform nanowires, but their pore density is significantly lower than anodized alumina. They are available commercially in various sizes. Their handling and template removal are also easier. However, the flexibility of these membranes may cause distortion due to heating [43].

One important criterion when conducting electrodeposition experiments is that template materials need to be compatible with the processing conditions. The pore size, porosity, morphology, chemical and thermal inertness are some of the properties of the templates that need to be considered. Another important issue is depositing material or the electrolyte solution must wet the internal pore walls for electrodeposition to take place. Otherwise, electrolyte solution will not penetrate the small pores and electrodeposition cannot be performed. Finally, growth mechanism of the fibers should be examined carefully to be able to have a control on the morphology of the product. For example, in order to synthesize nanowires/nanorods, the deposition must start from the bottom of the template along the pore opening whereas for nanotubes, the deposition should start from the pore walls and proceed radially inward [27].

2.3 Other applications of nanowires/nanotubes

Great progress has been made in different scientific areas with recent advances in nanotechnology with nanowires/nanotubes fabricated through different methods. These nanostructured materials with their unique physical and chemical properties have potential applications in industrial areas other than hydrogen storage such as cancer therapies, biosensors, hydrogen sensors, batteries, etc [44]. For example, it is well known that there are strong adverse effects with today's cancer therapies because healthy tissues in the vicinity of a tumor can be damaged during the treatment. Recently, it has been tried to use functionalized and biocompatible nanotubes by transferring these materials non-invasively to the deep layers of tissue in the human body. If materials with ferromagnetic properties are used, they can be placed precisely in the desired location by applying external magnetic field so that treatment can be done through these nanotubes by slow drug release or with some other methods [45].

Another exciting area is where the nanowires have been used is in MEMS based electrochemical biosensors. These biosensors have enormous importance in clinical investigations and may be used to determine cholesterol levels in blood. In a recent study, Au nanowires have been used in biosensors for estimation of total cholesterol in blood serum. The reason for using Au nanowires is to enhance the electron transfer between the enzymes and electrodes and hence increase the electrical conductivity and decrease the diffusion time due to large surface to volume ratio of these materials [46].

Large surface area of nanowires makes them efficient materials also for hydrogen sensors. It has been shown that hydrogen sensors utilizing palladium nanowires show better performance in detecting hydrogen concentration when compared to macroscopic

palladium sensors. Due to hydrogen incorporation, palladium nanowires swell and come closer which in turn reduces the electrical resistance. Therefore, palladium nanowire hydrogen sensors show faster response time due to reduced resistance which can be attributed to the large surface area of these materials [47].

2.4 Theory about electrochemical cells

An electrochemical cell is used to create voltage and current from chemical reactions. When a chemical reaction is caused by an external voltage it is called an electrochemical reaction. The transfer of electrons between atoms in chemical reactions leads to oxidation/reduction reactions, or broadly redox reactions. The loss of electrons from an atom is called oxidation while the gain of electrons by the atom is called reduction. Generally, redox reactions occur in a simultaneous manner such that one species is oxidized while the other one is reduced. However, in an electrochemical cell, the two reactions are spatially separated and electrons flow through an external circuit. Electrochemical cells have two electrodes namely, cathode and anode to facilitate electron transfer to and from the solution. Oxidation reaction takes place on the anode electrode while reduction reaction occurs on the cathode side. There are two types of electrochemical cells, galvanic and electrolytic [48-50].

The galvanic type electrochemical cell makes use of two dissimilar metal electrodes each immersed in the electrolyte solution. Redox reaction in a galvanic cell occurs spontaneously. The anode of a galvanic cell is negatively charged while the cathode is positively charged. The source of the cell's negative ions is the anode where

spontaneous oxidation occurs. Galvanic cell reactions supply energy which is used to do work such as with batteries and fuel cells.

The affinity of the electrode metals to oxidize or reduce in a specific electrolyte solution depends on the electrochemical potential which in turn varies with temperature, concentration of the electrolyte solution and pressure. Depending on the sum of electrochemical potential differences, anode electrode will undergo oxidation reaction while the cathode electrode will undergo reduction reaction. As a result of this, potential difference between two electrodes is produced in the cell. In order to have a complete circuit, there has to be a conduction bridge between the anode and cathode electrodes which can be provided by a porous membrane. This membrane prevents rapid mixing of the two electrolyte solutions but allows ions to diffuse through. A typical galvanic cell is shown in Figure 8.

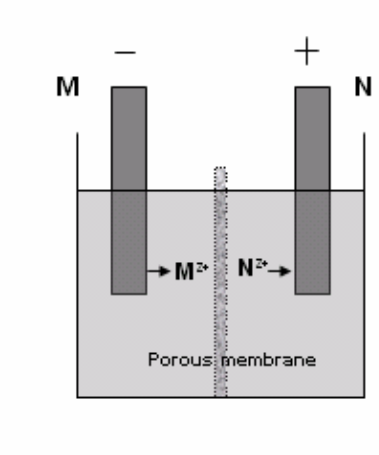

Figure 8. Galvanic Cell [51]

The half reactions taking place in a galvanic cell are;

$M \rightarrow M^{z+} + ze$ (oxidation reaction taking place in anode) [2]

$N^{z+} + ze \rightarrow N$ (reduction reaction taking place in cathode) [3]

and the overall reaction can be expressed as,

$M + N^{z+} \rightarrow M^{z+} + N$ [4]

The reactions can be started or stopped by connecting or disconnecting the external circuit. By the aid of an ammeter placed in the external circuit, the amount of electric charge that passes through the electrodes can be measured.

In contrast, non-spontaneous reactions occur in electrolytic cells. The anode of the electrolytic cells is positive because anode attracts ions from the solution. In both galvanic and electrolytic cells the flow of cations is from the anode to the cathode electrode. The reaction kinetics can be controlled externally by applying a potential difference between the electrodes in electrolytic cells. In this case, an external power supply helps to drive the electrode reactions. Electrolytic cells are composed of a vessel to do electrolysis containing electrolyte solution, anode and a cathode. The major difference of electrolytic cells from galvanic cells is that galvanic cells make use of two dissimilar metals separated from each other whereas electrolytic cells may use the same metal. Thus, electrolytic cells are driven by an external electrical charge with galvanostatic cells drive an external charge (electron) transfer. The schematic of a common electrolytic cell is shown in Figure 9.

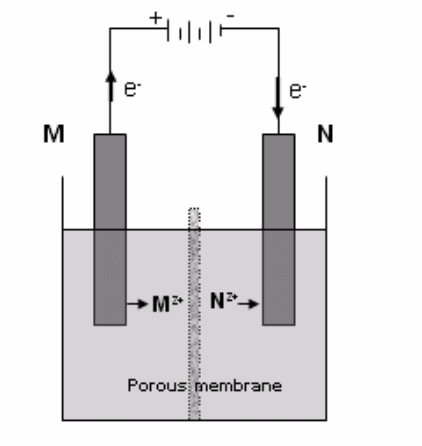

Figure 9. Electrolytic Cell [51]

In electrochemical cells, current is measured in amperes (A), and the potential across the two electrodes is measured in volts (V). Potential has units of J/C which can be explained as the energy (J) per amount of electric charge (C). This indicates that the cell potential is a measure of the energy of the reaction (oxidation/reduction) taking place in the cell. Cell potential also known as electromotive force (emf) can be considered as the sum of the half potentials resulting from oxidation and reduction reactions. Thus, cell potential can be written as:

$$E_{cell} = oxidation\ \ potential + reduction\ \ potential \qquad [5]$$

Oxidation potential of a half reaction is the negative of the reduction potential for the reverse of that reaction. Therefore, tabulating either of the half-cell potentials of the available electrodes gives information on the overall cell potential. A list of standard reduction potentials of some of the elements including palladium at 25 ^{o}C and at a pressure of 1 atm is given in Table 1 [51-52].

Table1. Electrochemical series of some elements [52]

Reaction	E^o/V
$PbSO_4 + 2e \Leftrightarrow Pb + SO_4^{2-}$	-0.3588
$PbSO_4 + 2e \Leftrightarrow Pb(Hg) + SO_4^{2-}$	-0.3505
$Pd^{2+} + 2e \Leftrightarrow Pd$	0.951
$[PdCl_4]^{2-} + 2e \Leftrightarrow Pd + 4Cl^-$	0.591
$[PdCl_6]^{2-} + 2e \Leftrightarrow [PdCl_4]^{2-} + 2Cl^-$	1.288
$Pd(OH)_2 + 2e \Leftrightarrow Pd + 2OH^-$	0.07
$Pm^{2+} + 2e \Leftrightarrow Pm$	-2.2
$Pm^{3+} + 3e \Leftrightarrow Pm$	-2.3
$Pm^{3+} + e \Leftrightarrow Pm^{2+}$	-2.6
$Po^{4+} + 2e \Leftrightarrow Po^{2+}$	0.9
$Po^{4+} + 4e \Leftrightarrow Po$	0.76

Each half cell potential is measured against a standard hydrogen electrode (SHE). The SHE is the universal reference for determining half cell potentials which is assigned to have zero potential. The potential of all other electrodes is reported relative to the standard hydrogen electrode. Because the true or absolute potentials cannot be measured, reduction potentials are defined according to the standard hydrogen electrode.

Standard reduction potential (E^o) is measured under standard conditions which is at 25^{o}C, a 1 M concentration for each ion participating in the reaction, a partial pressure of 1 atm for each gas that is part of the reaction, and metals in their pure state [48, 52]. However, conditions for real cells usually deviate significantly from the standard or equilibrium condition. In this case, Nernst equation relates the real cell potential to the standard potential by the expression:

$$E = E^0 - \frac{R*T}{z*F} * \ln\left(\frac{a_c}{a_o}\right) \quad [6]$$

Here, E is the cell potential at the given condition, E^o is the standard reduction potential, T is the temperature (25 ^oC), R is the universal gas constant, F is one faraday which is the amount of charge carried by one mole of electrons (96,487 coulombs/mole electron), z is the number of electrons used in the reaction, a_c is the activity of the ion at the electrode surface and a_o that of the bulk solution [48].

When there is no current flow, the forward and reverse electrode reactions occur at the same rate resulting in no net reaction. A cell at this condition which is at equilibrium and it is said to be at open circuit potential (OCP). When this equilibrium is disrupted by making the electrode as a part of an electrochemical cell through which current is flowing, either the forward or reverse reaction is occurring faster and there will be a difference between the new potential and the original one. This difference in potentials is called the overpotential.

$$\eta = E_{new} - E_{OCP} \quad [7]$$

In equation 7, E_{OCP} is the open cell potential which is the potential in the absence of current, E_{new} is the potential of the same electrode as a result of current flowing and hence η is the difference between these potentials which is the overpotential [48-50].

The over-potential is used to overcome the barriers developed within the electrochemical set-up due to the double layer and drives the electrode reactions. The over-potential also helps the diffusion of the metal ions at the solution metal interface and in the bulk of the solution. The double layer effect is usually significant at the anode to

push the ions into the solution while the reaction at the cathode is usually controlled by diffusion [48].

2.4.1 Determination of the amount of metal deposited at the cathode

Due to Faraday's law, the amount that is produced as a result of electrochemical reaction at the electrode is proportional to the quantity of charge passed through the electrochemical cell. Therefore, Faraday's law states that:

$$w = ZQ \quad [8]$$

where, w is the weight of the product, Z is the proportionality constant which is the electrochemical equivalent and Q is the amount of charge passed during the process. Q is the product of the current in amperes and t is the time in seconds,

$$Q = It \quad [9]$$

hence, weight can be expressed as:

$$w = ZIt \quad [10]$$

According to Faraday's law, a cell requires 96,487 coulombs of charges in order to produce one gram equivalent of a product at the electrode. One coulomb is the quantity of electric charge transported by the flow of one ampere for one second and 96, 487 is called the Faraday's constant.

Faraday constant can be calculated from:

$$F = N_A e \quad [11]$$

where, N_A is the Avagadro's number and e is the charge of a single electron.

One equivalent is the fraction of an atomic unit of reaction that corresponds to the transfer of one electron. In general, it is expressed as:

$$w_{eq} = \frac{A_{wt}}{n} \quad [12]$$

where, A_{wt} is the atomic weight of the metal deposited at the cathode and n is the number of electrons involved in the electrodeposition reaction.

As was stated previously, 96,487 coulombs are required to deposit an equivalent of a metal so from equation 6,

$$w_{eq} = 96{,}487Z \quad [13]$$

and therefore,

$$Z = \frac{w_{eq}}{F} \quad [14]$$

when equations 10 and 12 are combined, Z can be expressed as:

$$Z = \frac{A_{wt}}{nF} \quad [15]$$

and from equations 6 and 13, the amount of metal deposited at the cathode,w can be expressed as [48]:

$$w = ZQ = \frac{A_{wt}}{nF} Q \qquad [16]$$

CHAPTER III

EXPERIMENTAL

In this chapter, a detailed description of the materials and apparatus used in the experiments are presented. Also, experimental procedure and information on the characterization techniques are provided.

3.1 Materials

In the first part of the experiments, nanostructured metal nanowires and nanotubes were produced by electrochemical deposition process. In order to fabricate the metal fibers, three different types of templates were used: commercial anodized alumina membranes, lab-made anodized alumina membranes and commercial track-etched polycarbonate membranes in various sizes. The physical properties of the membranes are presented in Table 2.

Table 2. Physical properties of the templates used in the experiments

Membranes	Pore size (nm)	Pore density (cm^{-2})	Thickness (μm)	Aspect ratio (-)	Surface porosity (%)
Polycarbonate membrane	1,000	$2x10^7$	11	~11	~15.7
	100	$3x10^8$	6	~60	~2.4
	15	$6x10^8$	6	~400	~0.11
Commercial alumina	80-200	$1x10^9$	60	~300	~25-50
Lab-made alumina	60	$3x10^{10}$	80	~1300	~30

Commercial alumina and track-etched polycarbonate membranes used in this study were purchased from Whatman Corporation. Commercial alumina membranes have varying pore sizes from 100 to 200 nm and thickness of 60 μm. The porosity is within the range of 25-50%. The surface morphology of the commercial alumina membrane is presented in Figure 10.

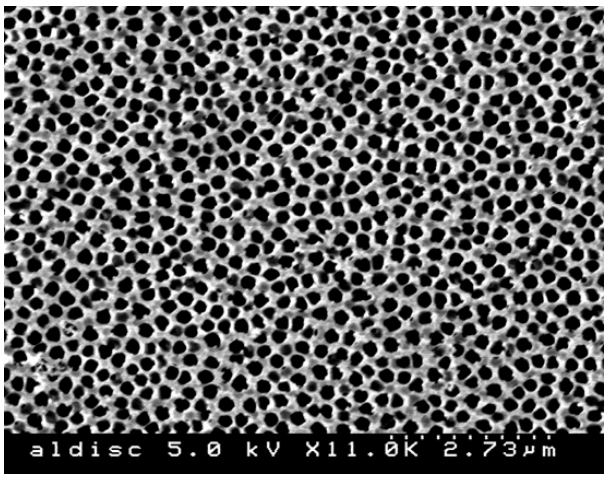

Figure 10. Representative SEM picture of commercial anodized alumina surface

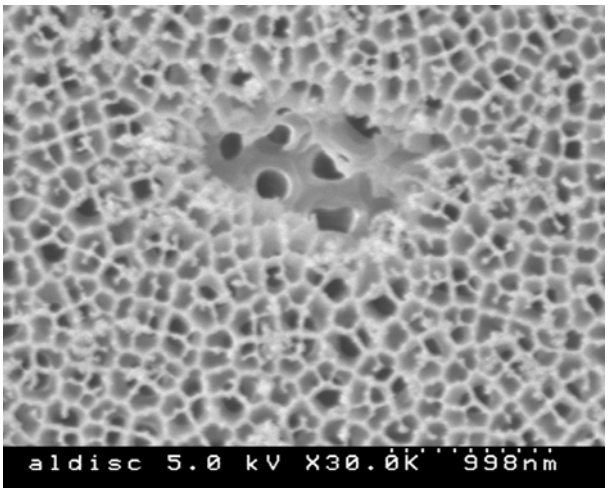

Figure 11. Other side of commercial alumina membrane

As was examined by SEM (scanning electron microscopy) commercial alumina membranes do not have uniform pore channels. There is branching of the pores throughout the thickness of the membrane (Figures 11 and 12).

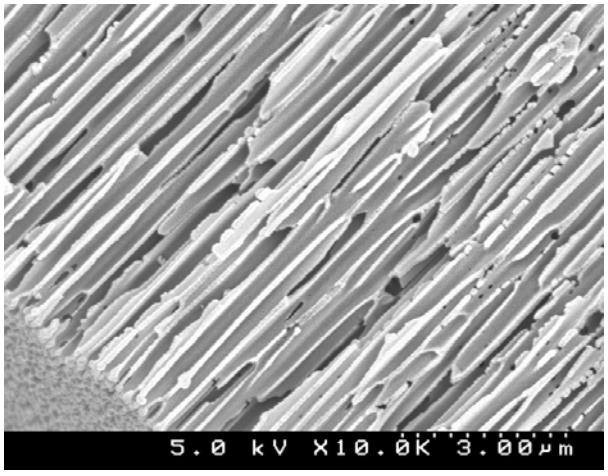

Figure 12. Cross-section of commercial anodized alumina

On the other hand, lab-made anodized alumina membranes have uniform pore size of 60 nm throughout the thickness of about 80 μm. Lab-made anodized alumina membrane was prepared by a co-worker, Pradeep Kodumuri. Briefly, 1 mm thick discs were cut from aluminum metal and polished mechanically to obtain a smooth surface using emery paper. After cleaning ultrasonically with soap, acetone and ethanol, the discs were electropolished for about 20 seconds. Then the electropolished metal was anodized at 40 V in 0.3 M oxalic acid for 24 hours. The remaining metal was dissolved away using $CuCl_2$ solution; 10% HCl and 0.3 M $CuCl_2$. Finally, the pore caps (oxide barrier layer) that form at the bottom of the pores were opened with 5wt % of phosphoric acid. The SEM picture of the lab-made anodized alumina is shown in Figure 13.

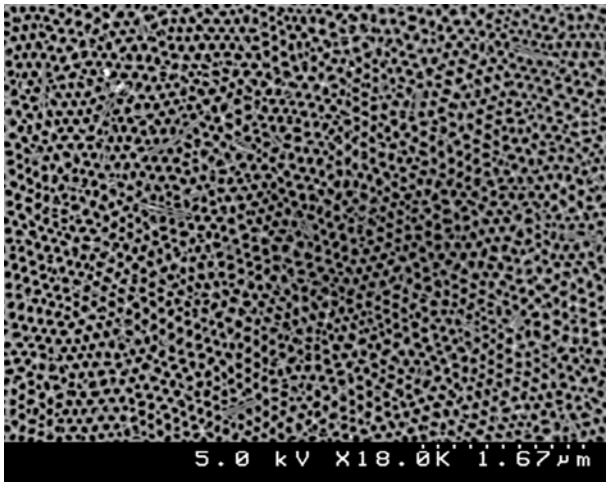

Figure 13. Lab-made anodized alumina surface

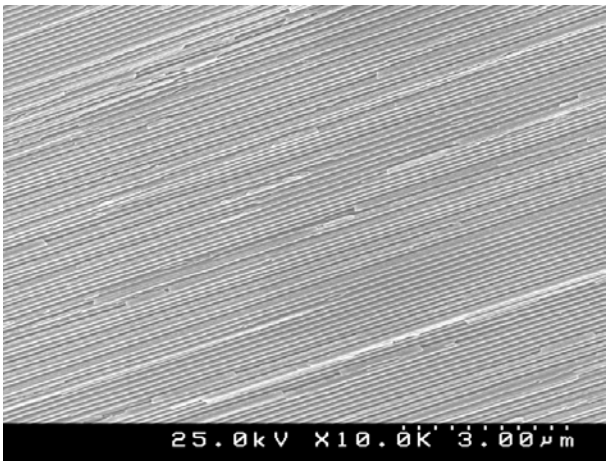

Figure 14. Cross-section of lab-made anodized alumina

SEM characterization technique showed that lab-made alumina has uniform straight pores (Figure 14).

The last class of template used in growing metal nanofibers is commercial track-etched polycarbonate membranes with three different pore sizes of 1,000 nm, 100 nm and 15 nm. The corresponding thicknesses are 6 μm for membranes with 100 and 15 nm pore diameters while it is 11 μm for 1,000 nm pore diameter membranes. Representative SEM pictures for the polycarbonate membranes are shown in Figures 15, 16 and 17.

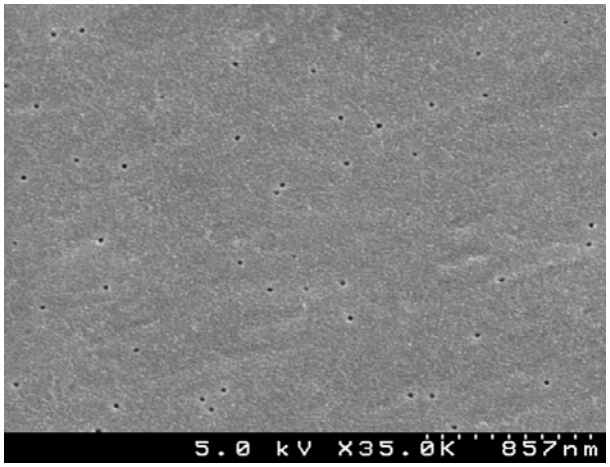

Figure 15. Polycarbonate track etched membrane with 15 nm diameter

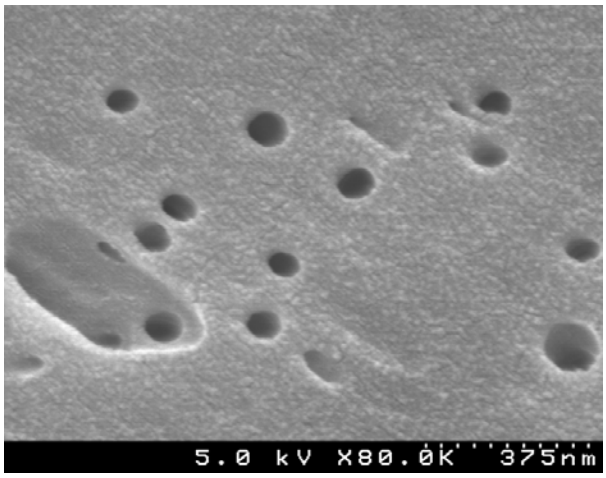

Figure 16. Polycarbonate track etched membrane with 100 nm diameter

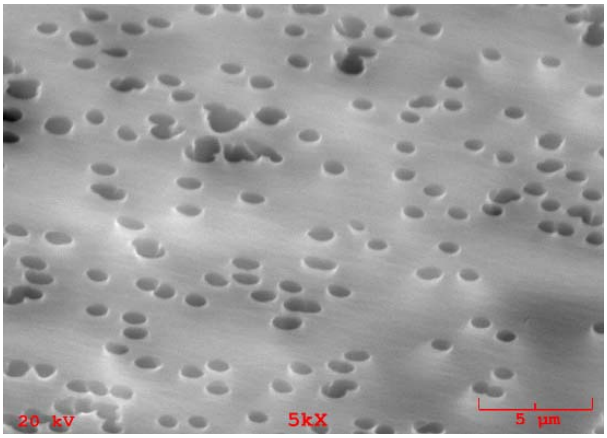

Figure 17. Polycarbonate track etched membrane with 1,000 nm diameter

Surface porosity of the polycarbonate membranes is the highest with 1,000 nm pore size membranes while lowest for the 15 nm membranes. Their pore densities are $2x10^7$, $3x10^8$ and $6x10^8$ cm^{-2} for 1,000, 100 and 15 nm pore size polycarbonate membranes, respectively. Furthermore, as can be seen from the SEM pictures the porosity of the polycarbonate membranes is significantly lower than the anodized alumina membranes. The porosity of the anodized alumina membranes varies from 25 to 50% and their pore densities are $1x10^9$ and $3x10^{10}/cm^2$ for commercial and lab-made anodized alumina membranes, respectively (Table 1).

3.2 Apparatus and experimental procedure for electrodepostion

Electrochemical deposition experiments were conducted to grow palladium nanofibers for later determination of their hydrogen sorption capacities by conducting equilibrium sorption experiments. In order to determine the optimum conditions and tune the electrodeposition process, nickel was used as the test metal before expensive palladium experiments.

3.2.1 Electrochemical deposition apparatus

Electrochemical cell used in our study is illustrated in Figure 18. This set-up used for electrodeposition consists of two electrodes, electrolyte solution and an external power supply.

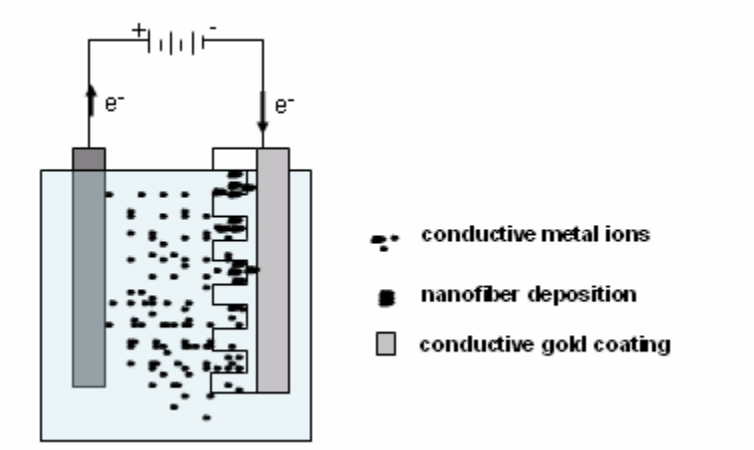

Figure 18. Electrochemical cell used in the present study

During the process of electrodeposition, electric current was applied across an electrolyte solution in which a substance was deposited at one of the electrodes. Electrolyte in this system helps to carry the current by means of ions. Positively charged ions are attracted to the negatively charged cathode while the negatively charged ions travel toward the positively charged anode. The charges of the ions are then neutralized by the charges on the electrodes and the products appear at the electrodes. The cathode is the target for electrochemical deposition and it is where metal deposits are produced. The electrode connected with the negative pole of the direct current source is the cathode. The

electrode connected with the positive terminal of the direct current source is the anode, the source of metal cations where the negatively charged ions, the anions, migrate. Direct current (DC) was applied between the terminals and the conditions of the experiment were adjusted according to the type of the application whether it is potentiostatic or galvanostatic electrodeposition.

A Solartron 1280B electrochemical test system was used as the power source and data acquisition system for conducting the electrodeposition experiments. The device can be adjusted to run both potentiostatic and galvanostatic experiments. The working electrode (WE) is connected to the anode and counter electrode (CE) is connected to the cathode. The current through the cell is measured between WE and CE.

Figure 19 shows the schematic diagram of the cell set-up connected to the power supply. It shows the anode (either nickel or palladium sheet depending on the type of fiber required to produce), the cathode which is the porous membrane supported by a metal sheet and electrolyte solution. The power supply is connected to a computer to monitor the data and control the experiment.

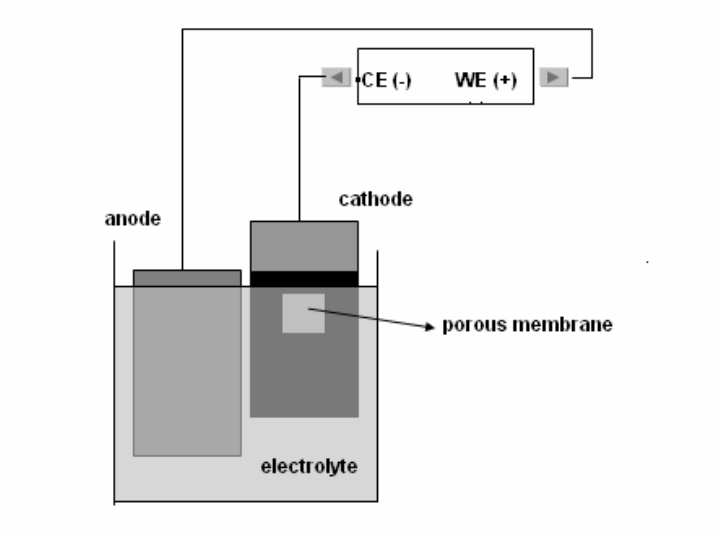

Figure 19. Electrochemical set-up used in the present study

In order to have a closer look at the cathode side of the system, Figure 20 is presented where the diffusing metal cations start forming the nanowires at the pore bottom through the pore opening.

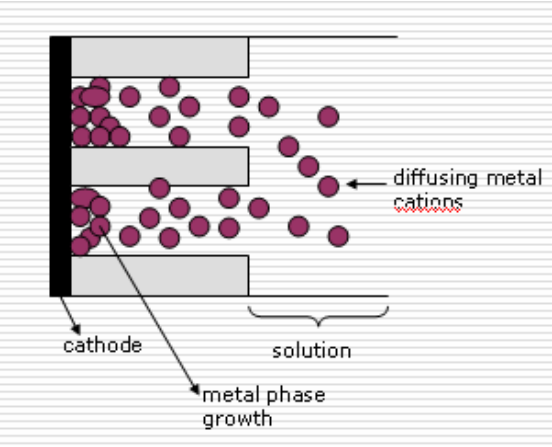

Figure 20. Nanowire growth starting at the pore bottom and continuing in the pore direction in a bottom-up fashion

3.2.2 Nickel Electrodeposition Experiments

Nickel nanostructured materials were grown in various porous membranes. Initially, the experiments were conducted with track-etched polycarbonate membranes with various pore sizes. The process begins with sputtering one side of the membrane with gold of 30 nm in a SPI™ sputter. Then the gold coated side of the membrane is placed on a copper sheet which constitutes the cathode of the set-up. The copper sheet is flattened with the aid of a cylindrical object to provide better conductance with the polycarbonate substrate. A few drops of water were added on the membrane to promote its adhesion to the copper sheet and care was exercised to prevent trapped air bubbles.

The anode was composed of a nickel sheet of 5 cm x 5 cm dimensions with a thickness of 0.5 mm and purity of 99.98 %. It was purchased from Sigma-Aldrich. The electrolyte solution used was composed of 53.6 g/L of $NiSO_4.6H_2O$ and 30 g/L of H_3BO_3 as stabilizer so that the pH of the solution was between 3 and 4. The distance between the anode and the cathode was kept at 2 cm at all times. Deionized water with 18 MΩ.cm resistivity was used to prepare the solution. Galvanostatic electrodeposition was performed with a constant current density of 10 mA/cm^2 corresponding to ≈ 2-3 V potential at varying deposition times. Experiments were also conducted at higher current densities of 50, 100 and 200 mA/cm^2 to determine the effect of current density. All experiments were conducted at room temperature. After deposition, the sample was washed thoroughly with deionized water. Dissolution of the polycarbonate support using dichloromethane (Cl_2CH_2) revealed the morphology of the nanostructure growth in membrane protruding from the surface for easy imaging. Finally, the morphology of

nickel nanostructures was characterized using optical microscope, SEM (scanning electron microscopy) and EDX (energy dispersive X-ray analysis).

The above described procedure was also used to grow nickel nanostructures in commercial and lab-made anodized alumina membranes, except for using gallium-indium coating to achieve conductance at the cathode instead of gold sputtering. Back side of the membrane was similarly sputtered in a SPI™ sputterer with gold of 30 nm thickness to maintain the electrical connection between the power supply and the membrane. All experiments were conducted at room temperature and in the same electrolyte solution which was replaced frequently. The distance between the anode and the cathode was kept at 2 cm at all times. The applied current density was 10 mA/cm^2 for the alumina membranes. After deposition, the alumina membranes were dissolved in 6 M NaOH solution. Figure 21 represents a schematic of the metal nanowires grown in a nanoporous membrane.

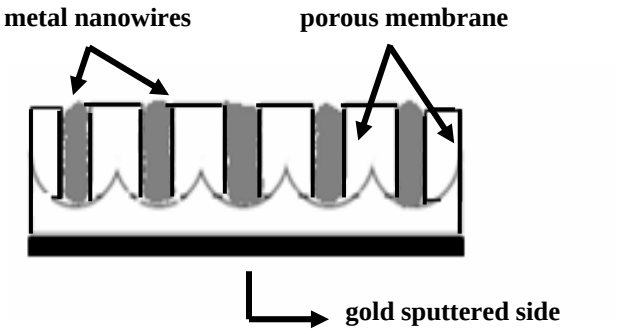

Figure 21. Schematic diagram of the procedure used to fabricate nickel nanowires

3.2.3 Palladium Electrodeposition Experiments

Palladium nanowires have been synthesized in 2 mM $PdCl_2$, 0.1 M HCl solution. Experiments were conducted at room temperature. Additives were not used to prepare the electrolyte solution to eliminate the presence of any other growth parameters. The back side of the membrane was gold sputtered to provide conductance of 30 nm thickness in a SPI™ sputter. Also silver paint instead of gallium-indium mixture was applied to this side to enhance the conductance. The membrane was placed on a copper sheet and used as the cathode (Figure 22).

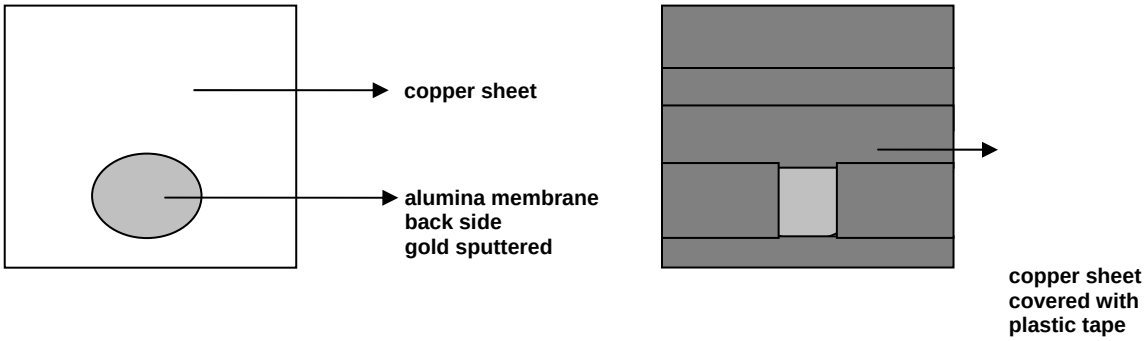

Figure 22. Schematic diagram of the cathode for palladium electrodeposition experiments

The anode was high purity palladium sheet of thickness 0.25 mm and purity > 99 %, with 5cm * 5cm dimensions purchased from Sigma-Aldrich. It was cleaned and degreased sequentially with soap, acetone and alcohol in an ultrasonic cleaner. Polishing and cleaning procedure was repeated at regular intervals as corrosion on anode was apparent. Deionised water with resistivity of 18 MΩ.cm was used to prepare the solutions

and also for cleaning the glassware used in the experiments. The deposition was carried out both potentiostatically and galvanostatically. In the experiments where potentiostatic deposition was carried out, a constant potential of 0.5 V was applied between the two electrodes. On the other hand, in galvanostatic experiments, the applied constant current density was 0.2 mA /cm^2 which yielded a corresponding steady-state potential of about 0.5-0.8 V. The amount of palladium deposited was controlled by the charge passed during deposition.

After deposition the sample was thoroughly washed with deionised water and dried in vacuum oven. Alumina membrane was dissolved in 6 M NaOH solution to get the free standing palladium nanowires. During the dissolving step membranes were also washed continuously to get rid of NaOH residuals from the membranes. After drying in vacuum oven, palladium nanowires were analyzed using optical microscope, SEM (scanning electron microscopy), EDX (energy dispersive x-ray analysis), optical microscopy.

Figure 23 shows a membrane after dissolved with NaOH solution mounted on a pedestal to perform the characterization studies with the previously cited devices.

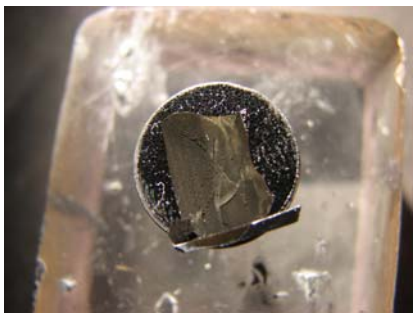

Figure 23. Palladium electrodeposited commercial membrane ready for SEM/EDX analysis

3.3 Volumetric System

In the second part of the experiments hydrogen sorption capacity of the produced nanowires was determined using a custom-made volumetric system. The physical properties of the gases used in volumetric experiments are shown in Table 3.

Table 3. Physical properties of the gases used in volumetric system experiments

Gas	Grade	% Purity	Supplier
Hydrogen	5	99.995	VNG
Helium	4.7	99.995	VNG

The schematic diagram of the volumetric set-up is shown in Figure 24. Afterwards, the detailed description of the experimental procedure and the protocol of how to conduct the hydrogen sorption experiments are presented in the following section.

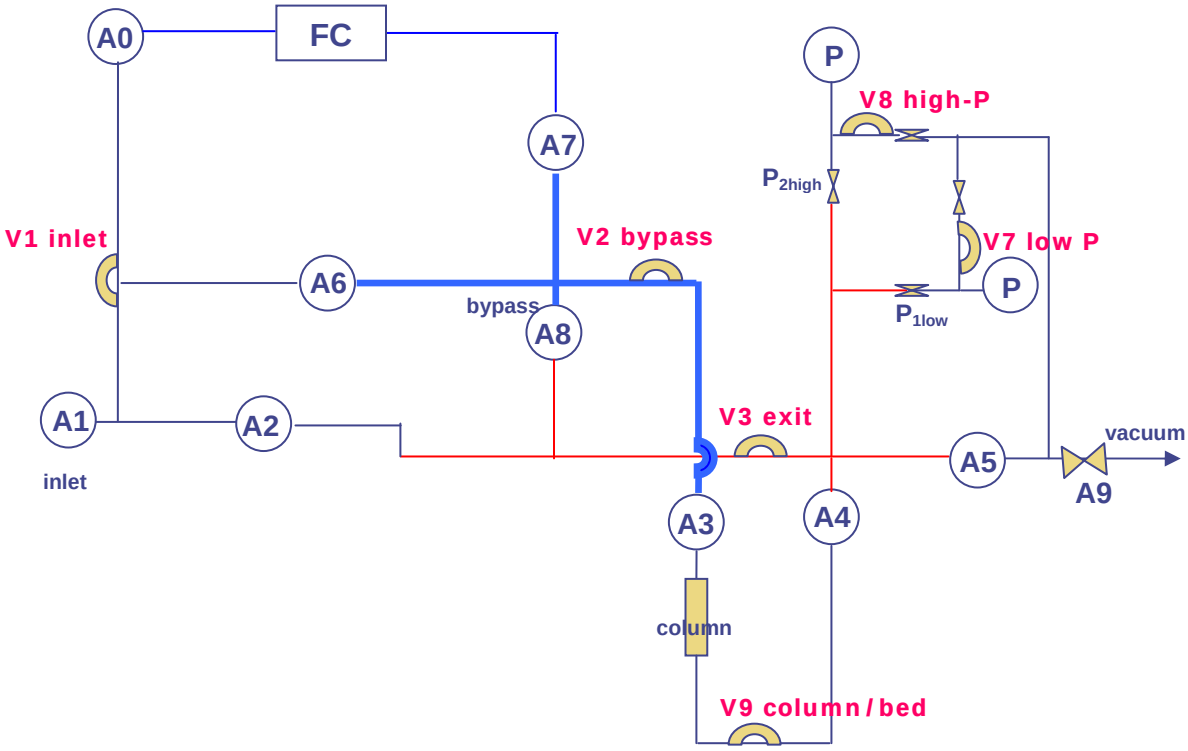

Figure 24. Volumetric system used to conduct hydrogen sorption experiments

About 55 mg of sample composed of membranes full of palladium nanowires was used in the experiments. A two-stage mechanical pump was used to remove impurities and moisture. The temperature of the sample chamber was controlled by the temperature controller. The volumetric set-up mainly consisted of an adsorption column, mass flow controller (FC), temperature controllers and high and low range pressure transducers. Helium gas was used to flush the system as well as to conduct the helium expansion measurements to determine the dead space in the system.

All lines used were stainless steel and ¼ inches outer diameter (O.D.), except sampling lines and pressure gauge lines which were 1/8 inches O.D. The sample was

introduced to the system with a 3-way flow control type valve. Pressure gauge valves (P1, P2, P3, P4) were H type compact rugged bellow valves. They were purchased from Nupro Company. The rest were all B type bellows valves, SS-4BK. Mass flow controller with model number FMA-2-DPV 1083 was purchased from Omega. Low pressure gauge with a pressure range of 0-15 psia with model number TGE/713-26 and high pressure gauge with a pressure range of 0-100 psia with model number TGE/713-10 were used in the experiments. Model number of the temperature controllers was CN 2011-J. Both pressure and temperature controllers were also purchased from Omega. All of the fittings used to construct the system were purchased from Swagelok.

3.3.1 Experimental procedure to conduct equilibrium hydrogen sorption experiments

Since hydrogen sorption experiments were conducted in a closed system, it is critical and important to know the system volume. Helium expansion method was employed in order to determine the volume of the system which has given quite accurate measurements. The principle is to expand helium gas from the unknown-volume section to the known-volume section or vice-versa. By using equation of state and material balances, the unknown volume can be calculated from the known volume. Another assumption considered in the calculations was that the helium gas was not adsorbed on solid walls of the system or on the metal samples. Determination of the known volume was crucial since it is the basis for hydrogen uptake of metal fibers. The material balances that were employed in volume determination of the system are shown in the appendix section in more detail.

The volume values of different sections in the system measured with helium expansion method are summarized in Table 3. The schematic diagram of the volumetric system is given in Figure 24 tagged with letters V describing the volumes in Table 4.

Table 4. Measured volumes of various parts of the volumetric system

Section	Description	Volume, cc	Method
INLET	V1	19.9662	Helium expansion
BYPASS	V2	9.9611	
EXIT	V3	14.4835	
LOW P	V7	8.139	
HIGH P	V8	6.8815	
COLUMN	V9	20.917	

The procedure for hydrogen sorption experiments is standard and consists of three steps: sample activation, adsorbate dosing and equilibration.

The sample was first activated by flowing hydrogen gas through the system at 200 ^{o}C for about 6 hours to get rid of any oxide formation from the surface of the material. After vacuuming the sample, temperature was increased to 300 ^{o}C and this time system was flushed with helium gas by the aid of a heating mantle around the sample chamber and under vacuum for overnight to get rid of the moisture and impurities from the system. At this time, A1 (inlet valve), A0 & A7 (FC valves), A3 and A4 (column valves to let the gas flow through the sample) and A5 (exit valve) were open, A6 & A8 (bypass valves) were closed. The mass flow controller was adjusted to approximately 11 cc/min. After activation process was completed, by using the mechanical pump, the system was evacuated. Then, the column was isolated from the rest of the system by closing valves

A3 and A4. A0, A7 and A5 were also closed and bypass valves, A6 and A8 were opened. The system was dosed with hydrogen gas by following the below stated protocol:

- Bring the 3-way valve to hydrogen position
- Open A1 (inlet) to let hydrogen gas in the system to the desired pressure. At this time, valves A6, A8 and $P1_{low}$, $P2_{high}$ are open to detect the pressure. When the dosed pressure is higher than atmospheric pressure, $P1_{low}$ is closed not to damage the low pressure gauge at high pressures. The rest of the valves are closed at this time.
- Close valves A1, A6 and A8 so the hydrogen gas is now trapped in V2 (bypass), V3 (exit volume), V7 and V8.
- After recording the column, ambient and jacket temperatures and the pressure, open valve A4 to let the hydrogen gas into the column.
- Wait until the thermal and pressure equilibrium is attained. Record all the measurements one more time.
- Close valve A4 and vacuum the system by opening valves A6, A8 and A5.
- Repeat the dosing and equilibrium steps until the desired pressure is reached.
- Mechanical pump (placed inside the fume hood) should run at all times to vacuum the system in between the dosing steps.
- When the experiment is over, vacuum the whole system and turn-off the pump and stop the temperature controller.

- Prepare the system for the next experiment by flowing He gas overnight with the previously mentioned method

3.4 Characterization

Optical microscope (Olympus BH2-UMA) and scanning electron microscopy (Amray 1820) devices were employed to determine the overall surface characteristics of the membranes before and after dissolving. Representative samples were cut from the samples and gold sputtered to provide conductance when imaging with SEM. Both sides of the membranes were examined in SEM at different magnifications.

Also, the chemical composition of the prepared samples was analyzed by energy-dispersive X-ray (EDX) spectrometry.

CHAPTER IV

RESULTS and DISCUSSION

4.1 Electrodeposition of nickel nanowires and nanotubes using various templates

In order to successfully grow palladium nanowires in the pores of the templates, electrochemical deposition experiments were first conducted with nickel as the model material for optimizing the conditions in fiber growth. Hence, several experiments were carried out with varying parameters to examine the growth mechanism of nanowires as well as nanotubes by the electrochemical deposition method.

Nickel nanotubes and nanowires were grown by galvanostatic electrodeposition in the pores of 1000, 100 and 15 nm polycarbonate as well as in commercial and lab-made anodized alumina membranes at a current density of 10 mA/cm^2. The effects of pore size, porosity, electrodeposition time, effective current density and pore aspect ratio were investigated.

4.1.1 Track-etched polycarbonate membranes

First part of the experiments was performed using track-etched polycarbonate membranes. Nickel hollow tubes were grown in 1,000 nm pore size track-etched polycarbonate membranes. These samples were composed of well-defined nickel hollow nanotubes that are about 4 μm long and have 1,000 nm outer diameter and 200 nm inner diameter (Figure 25). The membrane support (polycarbonate) was partially dissolved before SEM imaging to expose the tips of the nanotubes while holding the assembly together.

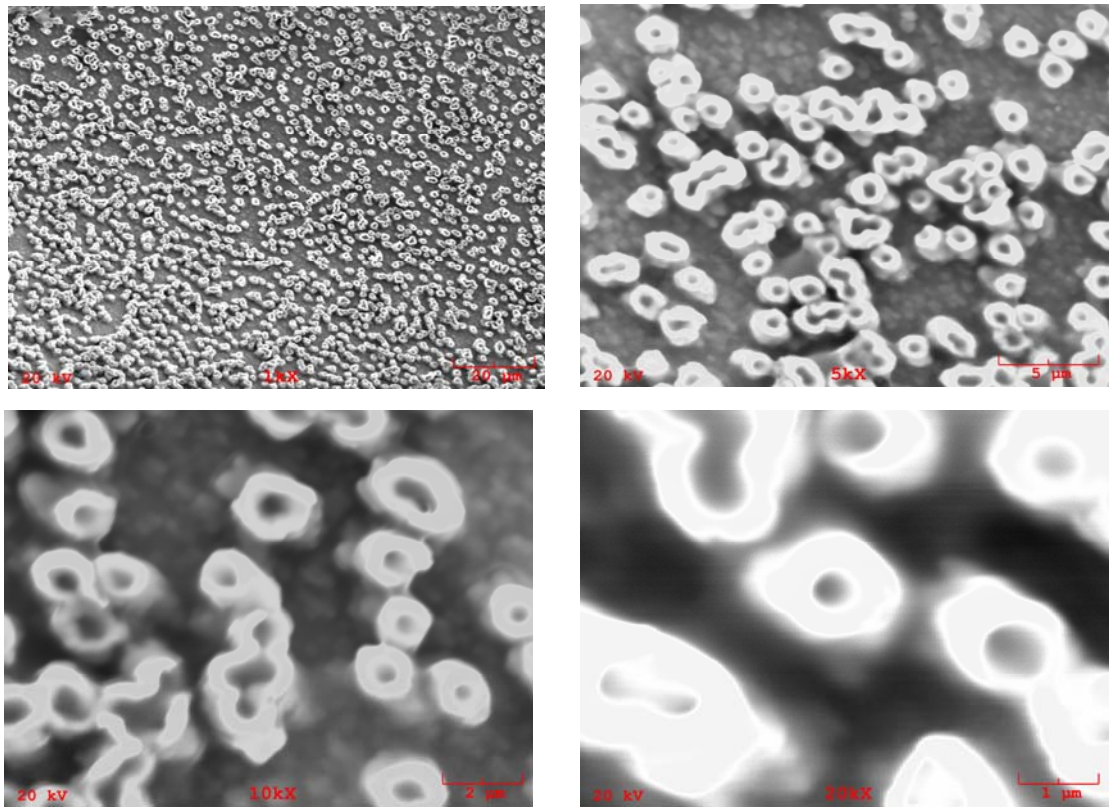

Figure 25. SEM micrographs showing nickel nanotubes deposited in 1,000 nm polycarbonate membrane partially dissolved with dichloromethane

Detailed examination of samples showed that deposition of nickel starts at the gold layer at the bottom circumference of the pores, and the nickel tubes grow along the pore wall to the top of the membrane. Preferred deposition along the pore wall surface may be due to the large surface area available providing energetically favorable sites for the adsorption of the metal ions before being reduced [53].

Table 5. (a) Representative EDX results of the nickel hollow nanotubes and (b) EDX analysis conditions

Elt.	Line	Intensity (c/s)	Atomic %	Conc. wt %
Ni	Ka	462.5	95.066	94.680
Cu	Ka	20.65	4.934	5.320
Total			100.000	100.000

(a)

kV	20.0
Takeoff angle	35.0°
Elapsed Livetime	100.00

(b)

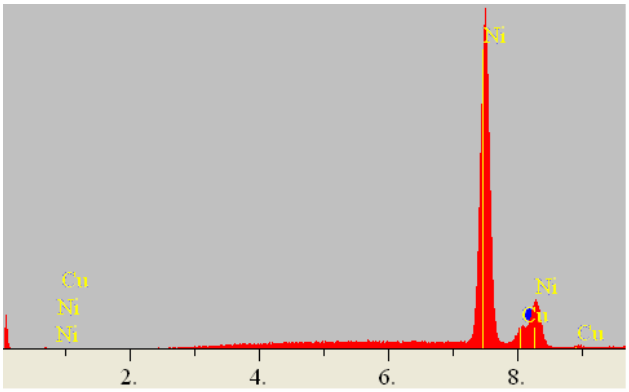

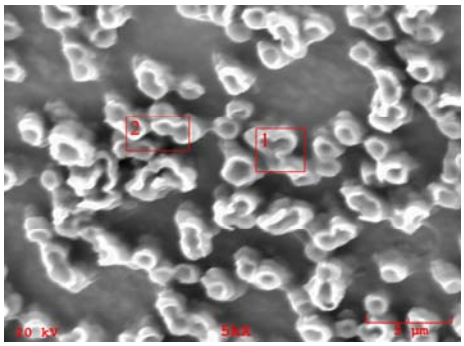

Figure 26. EDX spectrum of the nickel nanotubes

Table 5 represents the EDX analysis of the nickel nanotubes and it shows that approximately 95% of the composition is nickel while 5% is copper which comes from the copper metal sheet which was used as the support material for the membrane at the cathode. Figure 26 is the corresponding EDX spectrum of the nickel nanotubes. As can be seen, the major peak belongs to nickel making up the nanotubes.

These nanotubes were formed at early stages of the electrodeposition (Figure 25), corresponding to about 25 min of deposition time. Approximately, 15 C charge needs to pass to obtain the nanotubes at 10 mA/cm^2 current. At longer electrodeposition times, when the amount of charge increased to about 18 C, the nanotubes turned into nanorods (Figure 27).

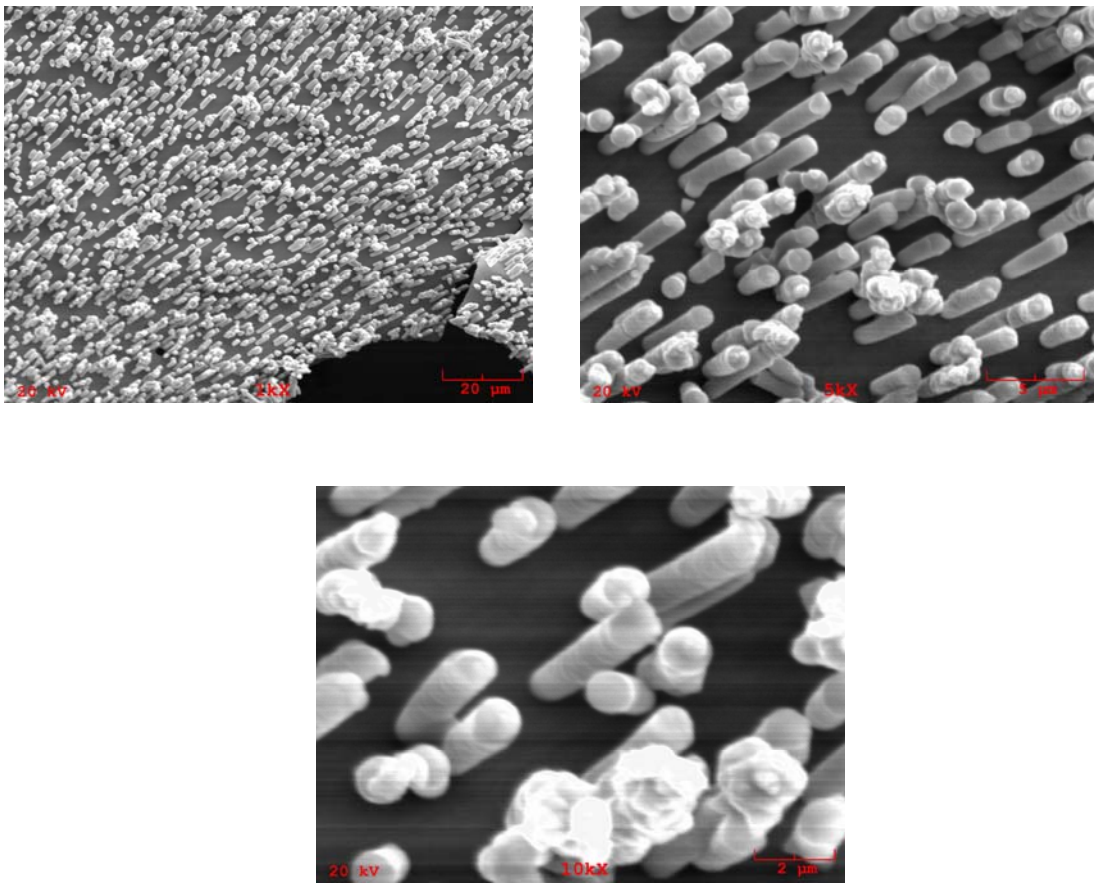

Figure 27. SEM micrographs showing nickel nanorods deposited in 1,000 nm polycarbonate membrane dissolved with dichloromethane at a longer time

Figure 27 also show that the metal deposition in the membranes are nearly perpendicular to the membrane surface, i.e. the heights of the fibers are constant indicating a uniform nickel growth in each pore of the membrane. Once the pores are completely filled with nickel, further electrodeposition produces hemispherical caps on the membrane surface, which subsequently merge together and result in a continuous overgrowth film (Figure 28).

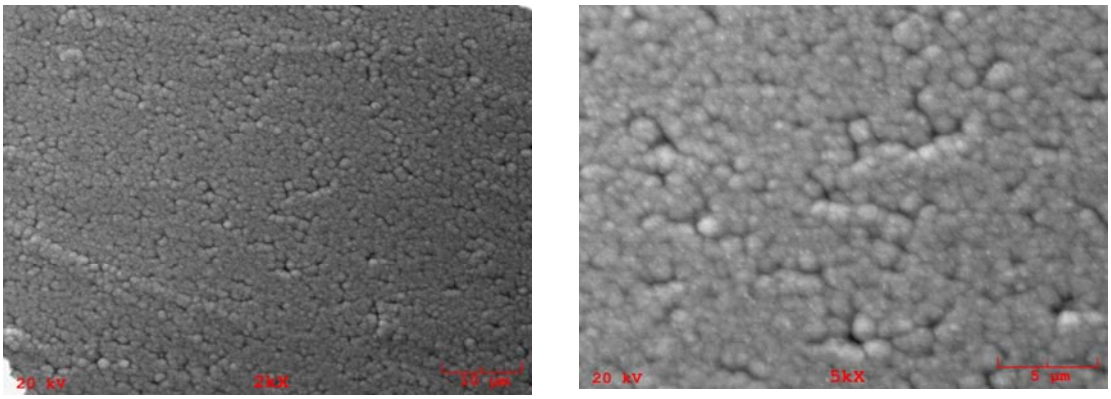

Figure 28. SEM micrographs showing nickel overgrowth on 1,000 nm polycarbonate membrane

Table 6. (a) Representative EDX results of the nickel overgrowth and (b) EDX analysis conditions

Elt.	Line	Intensity (c/s)	Atomic %	Conc. wt %
Ni	Ka	252.47	100.000	100.000
Total			100.000	100.000

(a)

kV	20.0
Takeoff angle	35.0°
Elapsed Livetime	100.00

(b)

Table 6 indicates that the continuous overgrowth film on the membrane is 100% nickel and its corresponding spectrum also shows the appropriate nickel peaks (Figure 29).

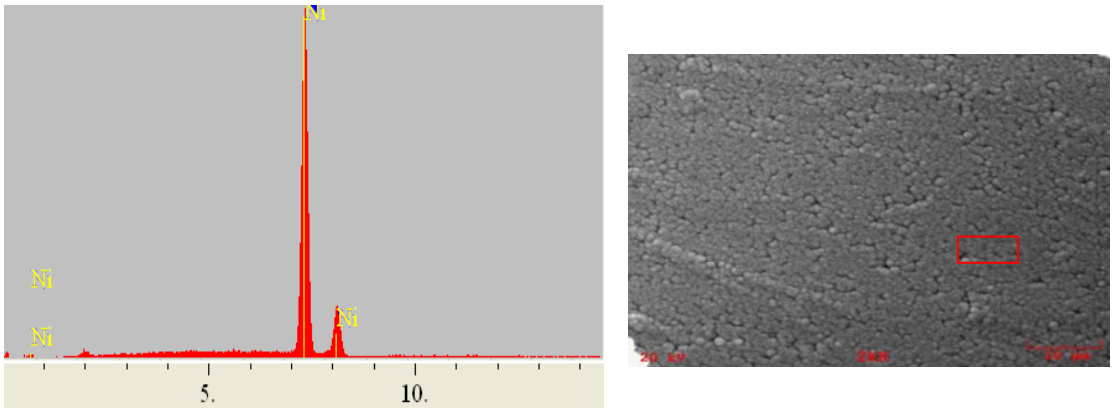

Figure 29. EDX spectrum of the nickel overgrowth film on polycarbonate membrane

The potential versus time graph of 1,000 nm polycarbonate membranes is presented in Figure 30 when a constant current density of 10 mA/cm^2 was applied. It can be seen that in all the three cases, corresponding potential was about 2.3 V as another indication of the reproducibility of the results.

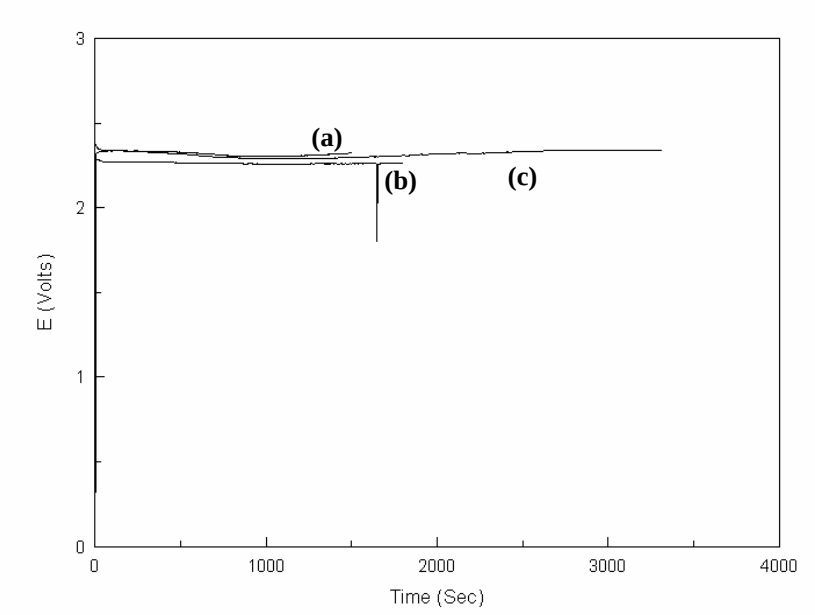

Figure 30. Potential versus time graph for the formation of nickel (a) hollow nanotubes (b) nanowires and (c) continuous overgrowth on 1,000 nm track-etched polycarbonate membranes

Figure 31 represents the graph of charge versus time for the same membrane. The charge is a straight line since the current was held constant during the experiments. Approximately, 15, 18, 32 C charge needs to pass in order to obtain the morphology of hollow nanotube, nanowire and continuous overgrowth, respectively.

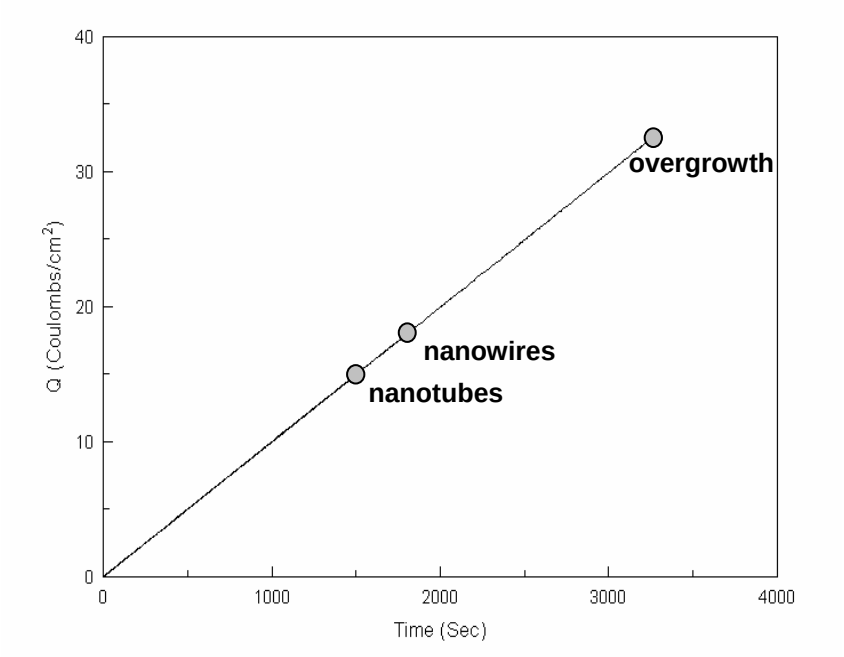

Figure 31. Charge versus time graph for the formation of hollow nanotubes, solid nanowires and continuous overgrowth film

Nickel fiber synthesis conditions for other studies are presented in Table 6 for comparison purposes. The effective current densities were calculated and listed based on pore density and pore diameter in order to eliminate the effect of non-conducting, non-porous membrane area on current density. It is interesting to note that Xue et al., 2006 were only able to obtain nanotubes in polycarbonate membranes by using pore-wall-modifying agents and increasing the voltage, and not by decreasing the deposition time. They obtained nickel nanowires when 12 mA/cm^2 effective current density was applied. The effective current density as high as 800 mA/cm^2 and wall-modifying agent were necessary to promote nucleation sites on the walls of the pores in order to produce nanotubes. It was also shown by other groups that nickel nanotubes can be produced at very low current densities as long as wall-modifying agents are being used [28, 30]

(Table 7). However, chemical modification of the inner walls of the template introduces impurities to the system as well as complicating the process [53]. Here, nanotubes were synthesized with one-step electrochemical deposition without the need of modifying the inner walls of the templates which is a much simpler and straightforward approach.

Table 7. Pore characteristics of the templates used in this study and other studies

Membranes	**Pore size (nm)**	**Effective current density (mA/cm^2)**	**Pore density (cm^{-2})**	**Thickness (μm)**	**Aspect ratio**	**Surface porosity (%)**
Polycarbonate membrane (this study)	1,000	63.7 (hollow)	$2x10^7$	11	~11	~15.7
	100	417 (solid)	$3x10^8$	6	~60	~2.4
	15	9091(solid)	$6x10^8$	6	~400	~0.11
Commercial alumina (this study)	80-200	26.7 (solid)	$1x10^9$	60	~300	~25-50
Lab-made alumina (this study)	60	6.7 (solid)	$3x10^{10}$	80	~1300	~30
Polycarbonate (from reference 28)	400	12 (solid), 800 (hollow) with agent	$1x10^8$	6 to 10	~20	~12.5
Commercial alumina (from reference 30)	80-200	0.8 (hollow) with agent	$1x10^9$	60	~300	~25-50
Commercial alumina (from reference 54)	80-200	0.35(hollow) with triblock copolymer	$1x10^9$	60	~300	~25-50
Commercial alumina (from reference 55)	80-200	26.7 (solid)	$1x10^9$	60	~300	~25-50

Current density of 10 mA/cm^2 was also applied to smaller pore size polycarbonate membranes to see the effect of pore size, porosity and hence effective current density. Normally hollow nanotubes have a tendency to grow in higher current densities. Slow growth with low current density yield to solid nanorods [28, 32, 53].

As can be seen in Table 7, the effective current density increases with decreasing pore size which should normally result in nanotubes, not in nanorods. However instead of

nanotubes, we obtained solid rods for 100 and 15 nm polycarbonate membranes regardless of the high effective current densities (Figures 32 and Figure 33).

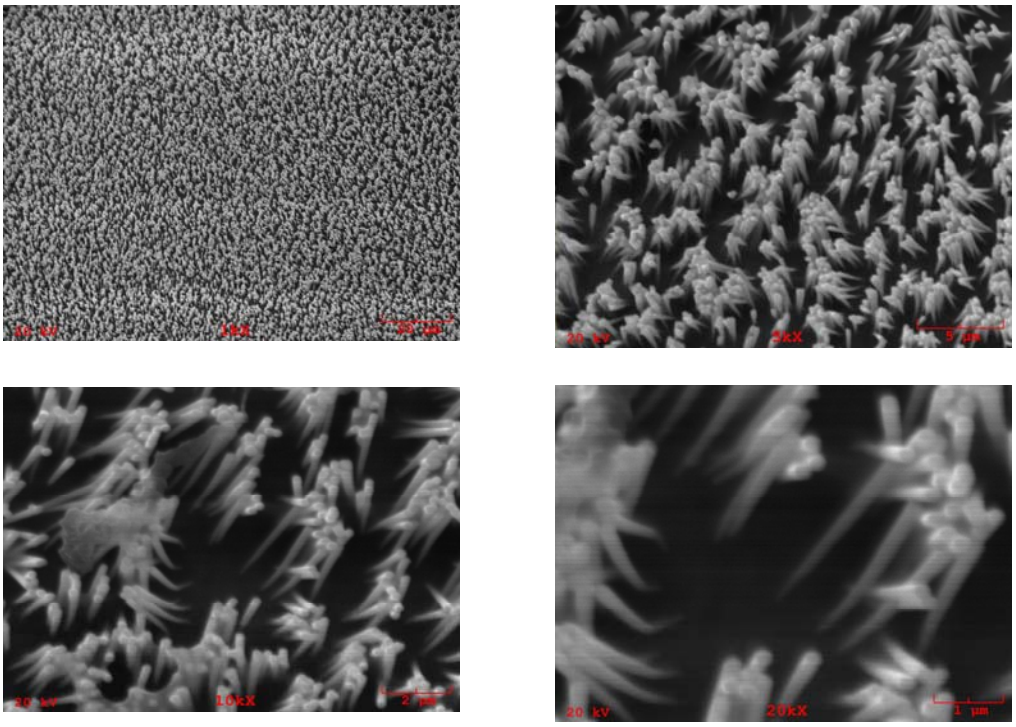

Figure 32. SEM micrographs showing nickel solid rods deposited in 100 nm polycarbonate membranes partially dissolved with dichloromethane

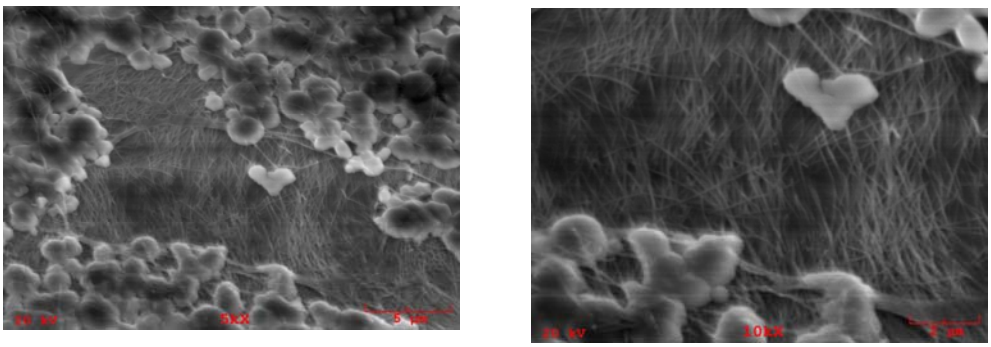

Figure 33. SEM micrographs showing nickel solid rods deposited in 15 nm polycarbonate membranes partially dissolved with dichloromethane

Based on this observation, we believe that the pore size has a dominant effect over effective current density in controlling the structure of the nanometals below a certain size.

Last parameter that has an effect on the structures of the templated nanostructures is the aspect ratio which is defined as the length over diameter ratio. It has been reported in literature that high aspect ratio membranes favor the formation of nanowires [56-57]. In our study, we obtained nanowires/nanorods for templates with aspect ratios of 60 and higher whereas hollow nanotubes were formed at much lower aspect ratios, around 11. Although preferential growth mechanism depends on effective current density, we believe that under a critical pore size solid rods will be formed if high aspect ratio templates are used. Deep and narrow pores promote layer by layer growth of nanorods. In contrast, in larger pore sizes, the metal can grow on the inner wall of the pores and form nanotubes. Thus, the resulting structure is determined by an intricate interplay between pore size (through effective current density) and aspect ratio.

Higher current densities such as 50, 100 and 200 mA/cm^2 were also applied to polycarbonate membranes to examine the effect. Solid rods were obtained instead of nanotubes in all cases. As was previously stated, the only condition that allows the formation of hollow fibers is with 1,000 nm polycarbonate membranes which eventually turn into solid rods with time. For the rest of the pore sizes, no matter what the current density was, nanowires were obtained.

4.1.2 Anodized alumina membranes

The second group of templates used was anodized alumina. A fixed current density of 10 mA/cm^2 was applied to anodized alumina membranes. For both commercial and lab-made alumina membranes only solid nanowires were obtained (Figures 34 and 35) supporting the previously stated discussions about aspect ratio and pore size.

As can be seen from Figure 34, the nanorods were grown to same height and were uniformly produced in each pore of the membrane. The diameter of the nanorods obtained in commercial alumina is around 200 nm which can be seen at high magnified SEM pictures, whereas much finer nickel fibers with 60 nm diameter were obtained for lab-made alumina (Figure 35), both determined by the pore size of the membranes. The density of these structures is orders of magnitude higher than polycarbonate grown nanorods in accordance with the much higher pore density of anodized alumina membranes. The high pore density of alumina membranes is in the range of 10^9-10^{10}/cm^2, therefore, the metal array stays together even after the alumina template is completely dissolved.

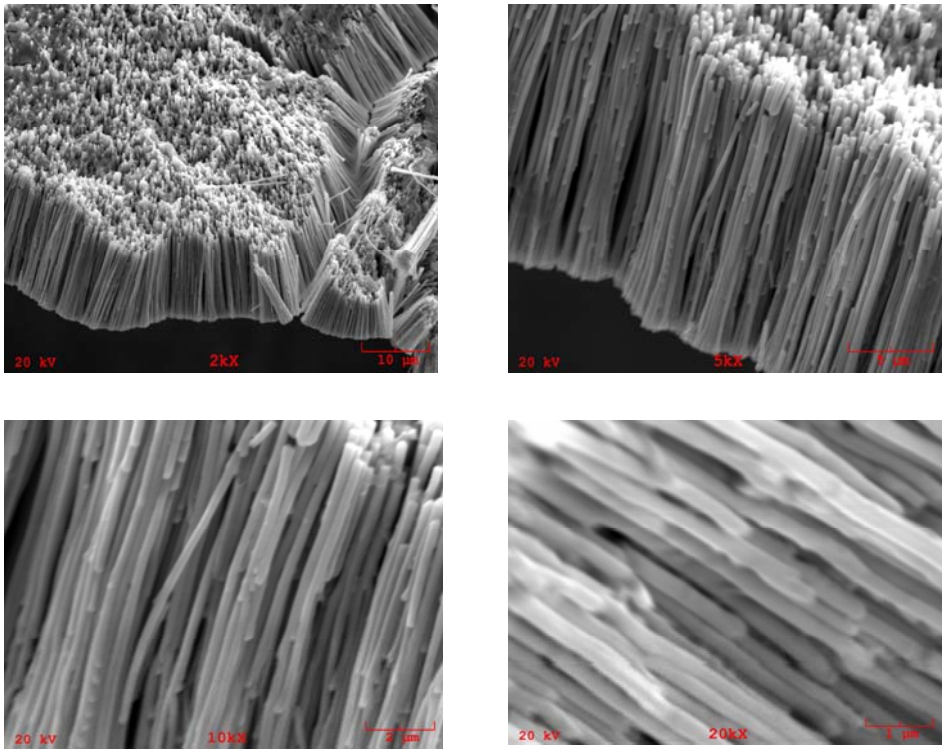

Figure 34. SEM micrographs showing nickel solid rods deposited in commercial alumina membranes dissolved with 6M NaOH solution

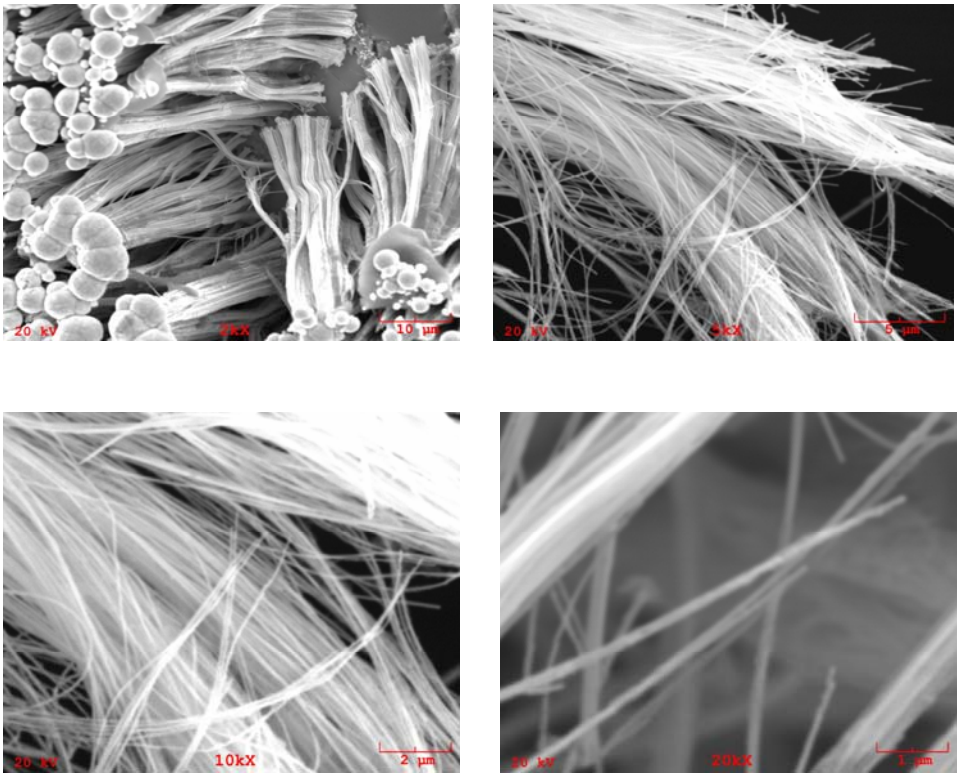

Figure 35. SEM micrographs showing nickel solid rods deposited on lab-made alumina membrane dissolved with NaOH solution. Overgrowth caps are visible on the upper left image

It is not expected to grow nanotubes with anodized alumina membranes which have high aspect ratio and high pore density resulting in lower effective current densities (Table 7). Both factors promote the growth of nanorods rather than nanotubes.

4.2 Electrodeposition of palladium nanowires using commercial alumina membrane

Palladium nanowires were synthesized using both potentiostatic and galvanostatic electrodeposition techniques in the pores of commercial anodized alumina membrane. Continuous, dense nanowire formation has been achieved with both techniques without any side treatment or further need of modification of the substrate being used.

Experiments were first conducted by using potentiostatic electrodeposition. In potentiostatic experiments, the applied potential range was varied from 0.5V to 3.5V while the electrolyte concentration was varied between 0.5 to 4 mM.

Table 8. The conditions applied for growing palladium nanowires

electrolyte concentration(mM)	applied potential (V)	appearance
0.5	0.5	brushing up of membrane walls X
2	0.5	nice, long fibers ✓
	0.8	overgrowth on the surface empty pores X
	1.5	loosely attached overgrowth X
	3.5	overgrowth on the surface empty pores X
4	0.5	overgrowth on the surface empty pores X
	2	overgrowth on the surface empty pores X

The parameters that have been tried for potentiostatic experiments at varying times can be seen in Table 8. When the electrolyte concentration was 0.5 mM with an applied potential of 0.5 V, the walls of the alumina membrane were brushed up which prevent the growth of nanowires inside the pores (Figure 36).

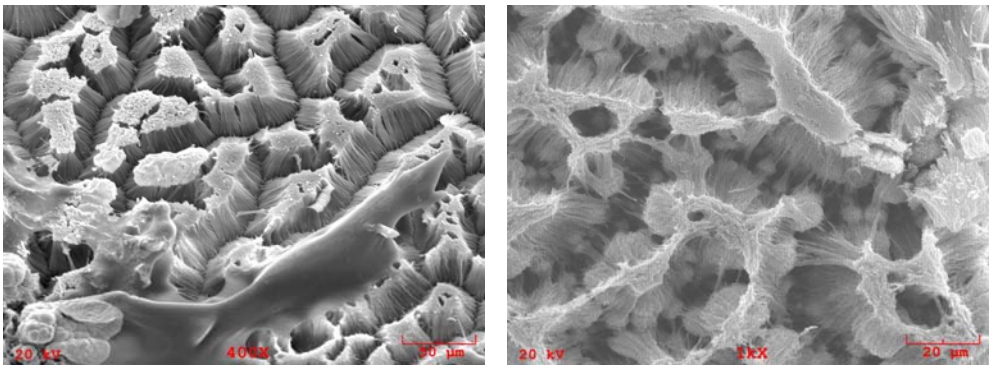

Figure 36. SEM micrographs of membranes with brushing-up morphology at an applied potential of 0.5 V with 0.5 mM electrolyte concentration

Increasing the electrolyte concentration to 2 and 4 mM at varying potentials resulted in obtaining overgrowth of palladium on the surface of the membrane. Detailed examination of the cross section of the membranes revealed that the pores of the membrane could not be filled completely (Figure 37). Same occurred with 2 mM electrolyte concentration at high potential differences.

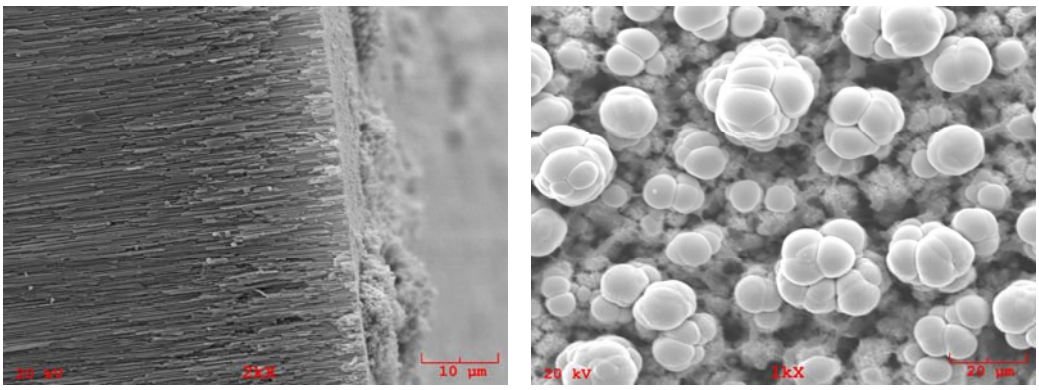

Figure 37. SEM micrographs of the membranes where the palladium was loosely attached on the surface and empty pores through the cross section at an applied potential of 1.5V with 2 mM (left figure) and dense overgrowth on the surface at an applied potential of 2V with 4 mM (right figure) electrolyte concentration

Palladium nanowires could only be obtained when 2 mM electrolyte concentration with an applied potential of 0.5V used in the experiments. As can be seen from the SEM images, there is dense and continuous nanowire growth along the membrane (Figure 38).

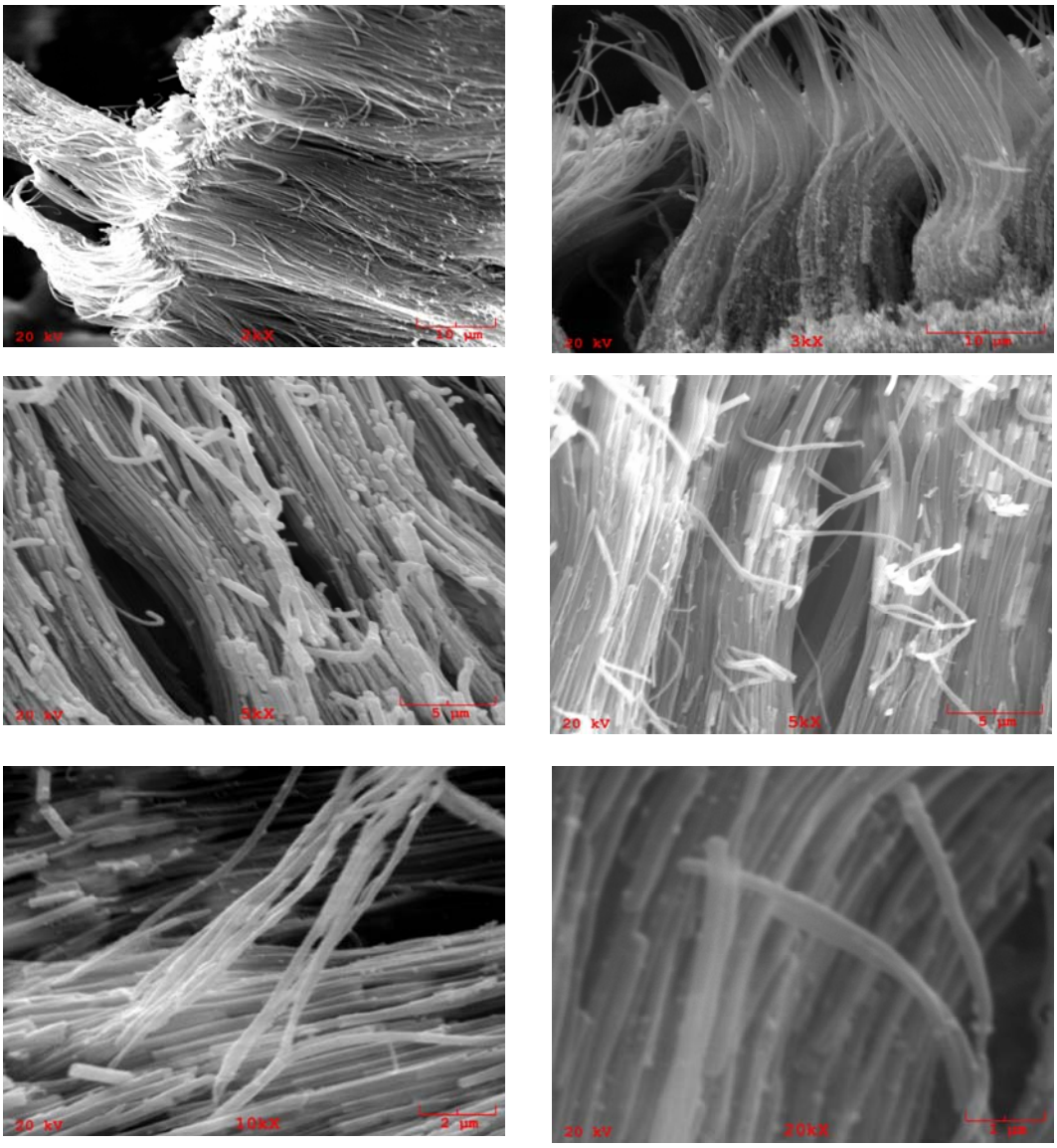

Figure 38. SEM micrographs showing palladium nanowires deposited in commercial alumina membranes (first two rows) and nanowires after the membranes partially dissolved with 6M NaOH solution (last row)

The deposition time at these conditions also was important to adjust. After conducting several experiments, the optimum time to grow palladium nanowires without

overgrowth on the membrane surface was about 2.5 hours. If electrodeposition was applied for extended times, continuous overgrowth film was observed on the membranes which is not desired for hydrogen sorption experiments because aggregated particles of palladium would obscure the nanostructuring effect in hydrogen sorption experiments.

The energy dispersive spectrometry of the palladium nanowires show that the major peaks belong to palladium. The minor peak which indicates the presence of gold originates from the gold sputtering process necessary for conductance in electrochemical deposition process. Finally, trace amount of aluminum comes from the remaining part of the membrane after etching (Figure 39).

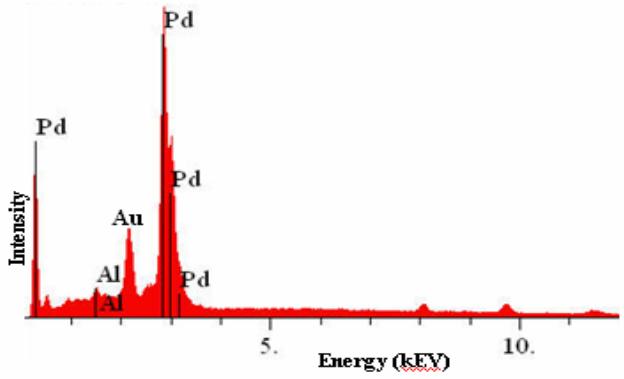

Figure 39. The corresponding energy dispersive spectrometry of the palladium nanowires

In order to confirm the reproducibility of results, the experiments were repeated by applying galvanostatic electrodeposition. Since the continuous and dense fibers were obtained at a potential of 0.5V with a corresponding current density of 0.2 mA/cm^2 in 2

mM electrolyte solution, galvanostatic experiments were conducted with a constant current density of 0.2 mA with the same solution concentration. As a result, continuous and dense nanowires were obtained with a corresponding steady-state potential within the range of 0.5-0.8 V. These results showed that, continuous palladium nanowires can be achieved by applying both potentiostatic and galvanostatic electrodeposition techniques with the indicated conditions. The potential versus time graph is presented in Figure 40 for palladium nanowires with galvanostatic electrodeposition experiments.

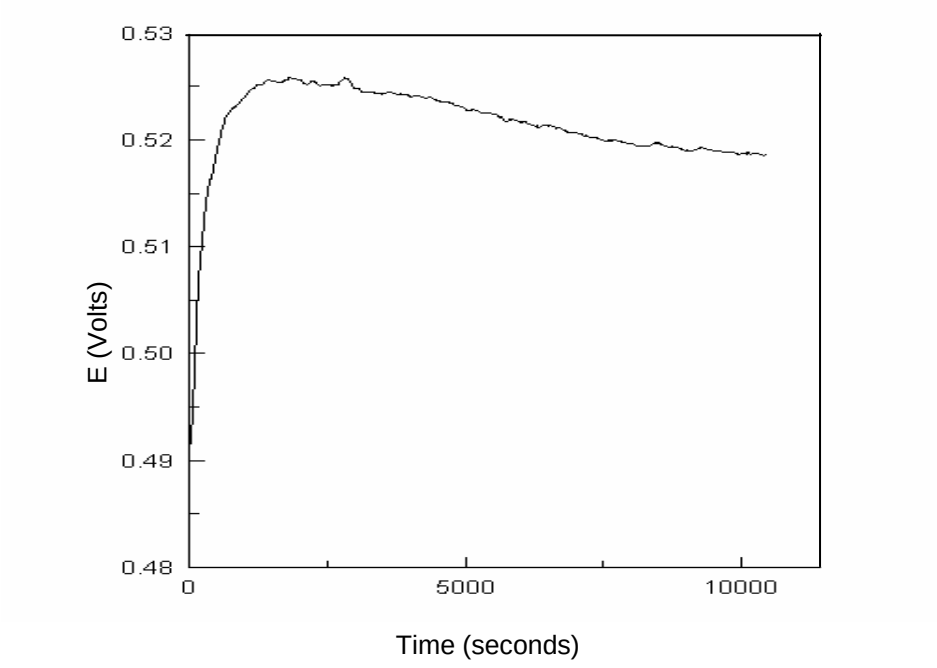

Figure 40. Potential versus time graph for the formation of palladium nanowires with galvanostatic experiments

4.3 Hydrogen sorption in nanostructured palladium

After obtaining palladium nanowires in the nanostructured pores of the membranes, hydrogen sorption experiments were conducted to determine the nanostructuring effect with these materials. This section summarizes the hydrogen sorption behavior of the self standing palladium nanowires as well as their behavior inside the membranes.

Palladium-hydrogen is a good model system to study the differences in hydrogen sorption behaviors between the bulk and the nanostructured materials since physical properties of bulk palladium are well characterized [20-22]. The experiments were first started with bulk palladium. This was necessary to test the custom-built apparatus and to compare the results with literature. The hydrogen sorption behavior of bulk palladium was investigated by the measurement of pressure-composition (P-C) isotherms using the custom-built volumetric system. Before hydrogen sorption measurements, it is crucial to pre-treat the system with hydrogen. Hydrogen treatment helps to remove any oxide formation from the surface of the samples due to easy decomposition of palladium oxide. For pre-treatment, the samples in the column were exposed to hydrogen at high temperature (200 ^{o}C) for about 6 hours. This allows larger hydrogen solubility due to activation of the surface sites by removing the oxide layer. The next treatment before starting the sorption experiments is to flow helium through the system at 300 ^{o}C to desorp the sample completely and remove any pre-adsorbed moisture or impurities from the sample. Hence, experiments can be conducted with a clean palladium surface. The last step is to evacuate the system before starting the experiments.

4.3.1 Hydrogen sorption studies with bulk palladium

The experiments were conducted at 135 and 185 ^{o}C volumetrically to investigate the hydrogen uptake behavior of bulk palladium. Volumetric technique measures the amount of hydrogen absorbed by the metal at a fixed known volume by monitoring the pressure drop due to sorption [58].

Pressure-composition isotherms for the sorption of hydrogen by bulk palladium at two temperatures are given in Figure 41. The hydrogen solubility is given by molar concentrations of hydrogen per Pd atom for an equilibrium hydrogen pressure.

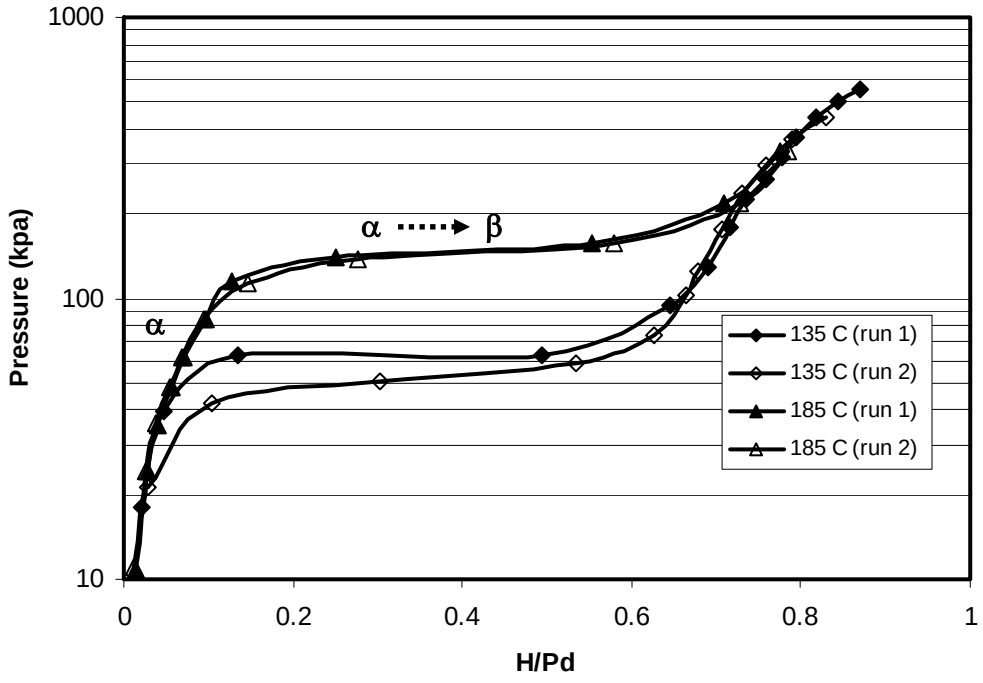

Figure 41. Hydrogen pressure-composition isotherms of bulk Pd at 135 ^{o}C and 185 ^{o}C

The figure shows that the P-C isotherm of the bulk material has three distinct parts. The initial steep slope at the low pressure range belongs to α phase where hydrogen dissolves and goes into solid solution. The solubility limit of this phase is around 0.15 H/Pd at both temperatures. The flat plateau which is also known as the miscibility gap that is present at both temperatures refers to the existence of two phases, α and β where the hydride phase starts to form. Upon the appearance of the hydride or the β-phase, the equilibrium pressure stays nearly constant as more hydrogen is added to the system. In this section, there is a rapid conversion of α phase into β phase as concentration of hydrogen increases. The flat plateau corresponds to about 60 kPa at 135 ^{o}C while it approximately corresponds to 150 kPa at 185 ^{o}C for H/Pd ratio of 0.4. As more hydrogen is added to the system second dissolution of hydrogen in the β-phase begins and the pressure rises again as a function of the hydrogen content.

Figure 42 presents the bulk palladium P-C isotherms obtained from this study and the study performed by Yamauchi et al., 2008 for comparison [21]. The two isotherms reveal similar plateau pressures. The flat plateau corresponds to about 62 kPa and 70 kPa for H/Pd ratio of 0.1 in this study and Yamauchi's study, respectively. The slight difference between the plateau pressures of the isotherms are due to the differences in temperatures at which the experiments are conducted. Hence, the isotherms from both studies confirm that our results are consistent with literature.

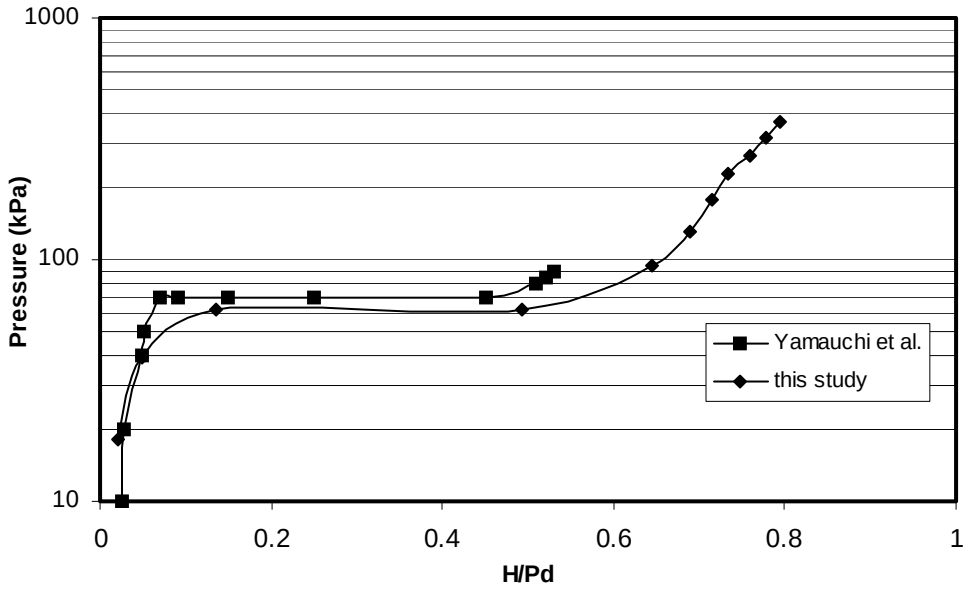

Figure 42. Comparison of the P-C isotherms of bulk palladium of this study (135 ^{o}C) and the study performed by Yamauchi et al., 2008 (120 ^{o}C)

4.3.2 Hydrogen sorption studies with palladium nanowires

The sorption behavior of the nanowires inside the membranes and the single standing nanowires after dissolving the membranes was investigated at both temperatures. After the membranes were dissolved with 6M NaOH solution, they were washed with distilled water to get rid of the residuals of NaOH and were dried after placed in the sorption column by gradually increasing the temperature up to 200 ^{o}C to remove the moisture. Then the routine procedure of pre-treatments similar to bulk palladium was also applied to palladium nanowires. In order to examine the effect of nanostructuring, the P-C isotherms of the nanowires before and after dissolving the membranes and the bulk palladium at 135 ^{o}C are plotted together for comparison (Figure 43).

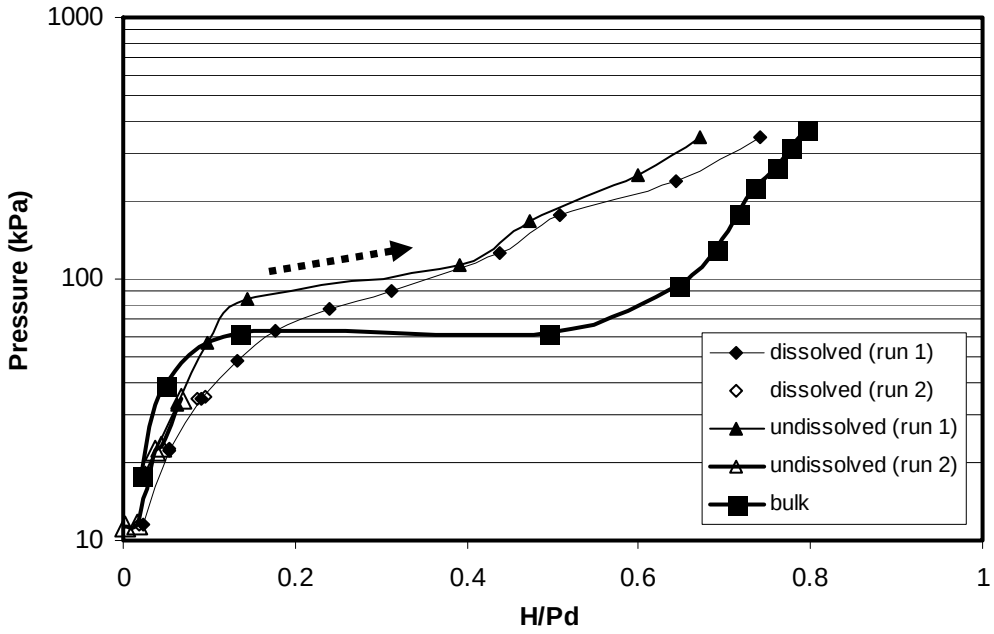

Figure 43. Hydrogen pressure-composition isotherms of Pd nanowires (before and after the membranes were dissolved) and bulk Pd at 135 ^{o}C

P-C isotherms in Figure 43 show that nanowires have isotherm shapes somewhat different than bulk palladium pressure-composition isotherm. The plateau is not well defined with nanowires, it slopes upward. Nevertheless, a "plateau-like" region is identifiable by the change in the slopes of the isotherms. This sloped plateau was observed approximately within the 0.15-0.4 range of H/Pd ratio for both dissolved and undissolved samples. The existence of the plateau-like region in both nanowires indicates that α and ß phases coexist as in the bulk phase and there is phase transformation. This phase transition occurs at different pressure levels unlike bulk palladium where the transition is at a fixed pressure. The width of this region was narrowed for both dissolved and undissolved samples when compared to bulk palladium.

In the low concentration region, up to α-phase with H/Pd ratio of about 0.15, nanowires show clearly higher sorption capacity than the bulk palladium. As the particle size is reduced, more adsorption sites for the hydrogen atoms are available due to the increase in the fraction of atoms occupying the surface and subsurface sites. Neutron scattering studies have also shown that nanostructured materials contain edges, corner sites, in other words, grain boundaries which create additional subsurface sites for hydrogen sorption [10]. Since monolayer hydrogen coverage already takes place on the surface, hydrogen atoms occupy the additional subsurface sites created by the grain boundaries and enhance the solubility of hydrogen in the α-phase (low concentration region) for nanostructured palladium. Therefore, there is an enhanced hydrogen uptake at low concentration region for both dissolved and undissolved samples. On the other hand, bulk material hydrogen dissolution is limited due to much lower number of subsurface sites [24,26].

There exists a reduced hydrogen uptake capacity for the nanowires when compared to bulk palladium, at high concentration region. The major reason for having lower hydrogen sorption is that the significant portion of the grain boundaries or subsurface sites may not have been transformed to the hydride phase [10]. Hence, these sites do not participate in hydride formation examined by neutron scattering studies which in turn decreases the sorption capacity at higher pressures [10,22]. Another reasonable explanation for the reduced capacity at higher pressures is attributed to the stress nanocrystals are exposed to at high pressure upon hydrogen loading as well as to the distribution in binding energies in different planes of the palladium [1]. It was determined that Pd nanograins revealed 1.3 and 2.4 % strain in the (111) and (100)

planes, respectively which will deform the lattice and reduce the effective volume for certain octahedron sites and hence, making the Pd nanograins less favorable for hydrogen atoms [59]. Therefore, strain hinders diffusion in the α-β boundaries and reduces the maximum hydrogen uptake capacity at higher pressures [1].

Dissolved and undissolved samples show similar trend in their hydrogen uptake behavior. The reason for dissolving away the membranes was to prevent the trapping of nanowires within the pores of the membrane, so to obtain single standing nanowires. When this barrier was removed more of the grain boundaries or defects of bare nanowires are exposed to hydrogen and therefore, contributes to slight enhancement of the storage capacity. Therefore, hydrogen sorption with dissolved samples is found to be slightly higher than the undissolved sample.

The storage capacities of the nanowires produced in these experiments reveal a storage capacity of about 0.7 wt% and generally fall within the range of the previously reported studies where they have used different methods for obtaining nanostructured palladium. For example, Kuji et al. have reported hydrogen storage capacities approximately 0.4 wt% for temperatures and pressures up to 398 K and 100 kPa, respectively [59]. Similarly, within the same temperature and pressure range, Yamauchi et al. have reported storage capacities as much as 0.5 wt% with the polymer coated nanostructured palladium synthesized by ethanol reduction of H_2PdCl_4 [60]. Furthermore, palladium nanoparticles produced by surfactant mediated single phase reduction synthesis have been reported to possess higher hydrogen adsorption capacities around 1 wt% but at a temperature of 298 K and at pressures an order of magnitude greater than that of the present study [8].

The hydrogen sorption experiments were also conducted at 185 ^{o}C for the bulk palladium and palladium nanowires. The hydrogen P-C isotherms of both nanowires and bulk sample at 185 ^{o}C are shown in Figure 44.

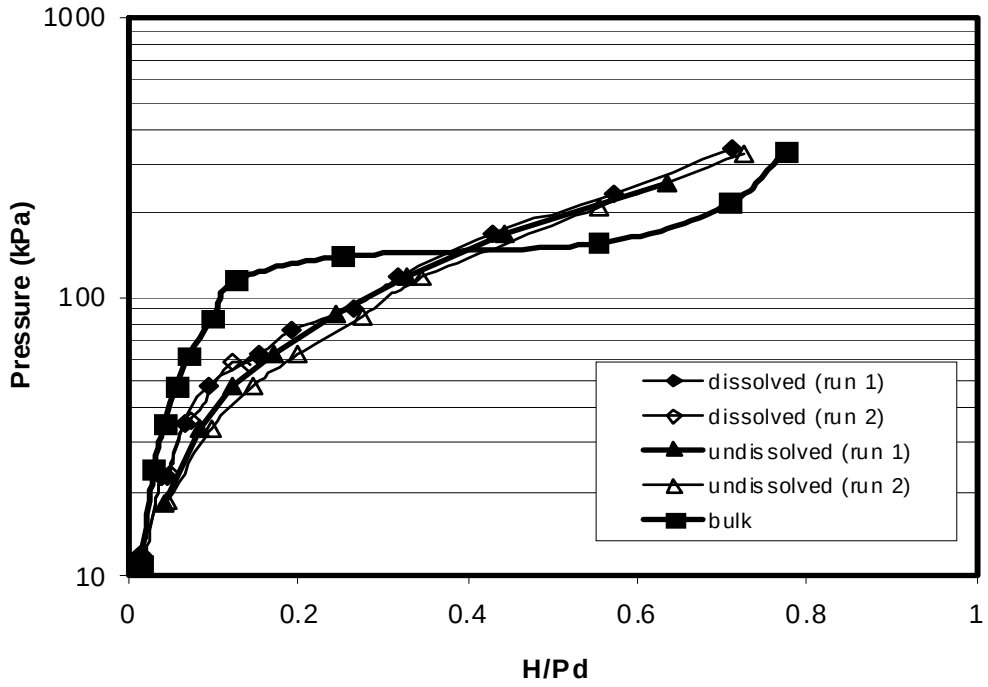

Figure 44. Hydrogen pressure-composition isotherms of Pd nanowires (before and after the membranes were dissolved) and bulk Pd at 185 ^{o}C

When the P-C isotherms of the three samples are investigated at 185 ^{o}C, the three distinct parts of the bulk palladium cannot be seen clearly with the palladium nanowires. Figure 44 shows that as the temperature increases, the plateau for the nanostructured materials starts to diminish and seems like only a single phase exists. This unique phase behavior that the nanostructured materials exhibit at high temperatures can be explained thermodynamically. As the temperature approaches to the critical temperature which is

about 160 ^{o}C for nanostructured [59] palladium, there is a significantly reduced phase transformation from α into β phase and eventually only single phase (α-phase) exists at and above the critical temperature.

Palladium nanowires show enhanced hydrogen uptake capacity in the α-phase also at this temperature and a reduced capacity at higher pressures. Furthermore, dissolved samples show similar hydrogen uptake capacity when compared to undissolved samples.

As was stated previously, hydrogen pre-treatment of the samples is important in order to remove any oxide formation on the surface of the samples. Figure 45 represents the isotherms of the hydrogen treated and untreated of the bulk palladium at 185 ^{o}C.

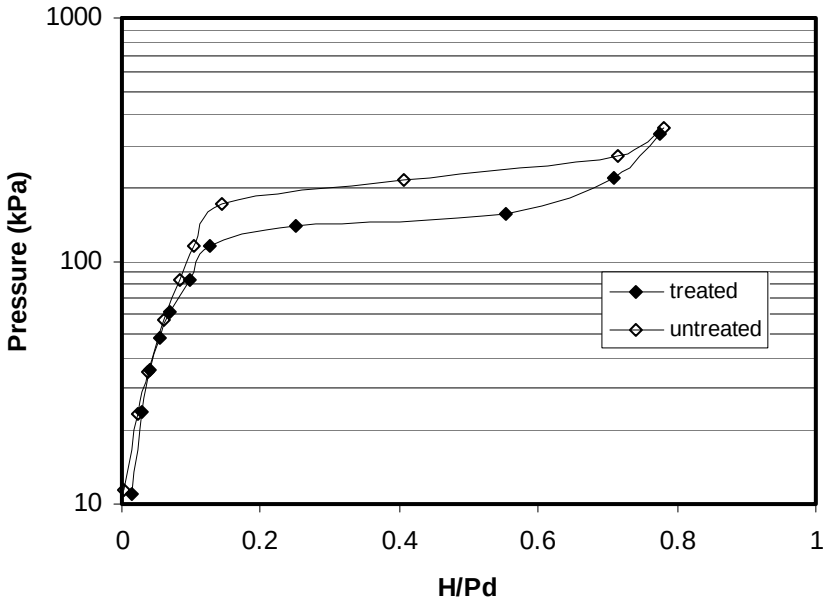

Figure 45. P-C isotherm of hydrogen treated and untreated bulk palladium sample at 185 ^{o}C

Figure 45 indicates that the hydrogen sorption capacity of bulk palladium sample is about 30% more than untreated sample. Hence, this shows that oxide formation on the surface of the samples needs to be removed with a pre-treatment method with hydrogen at high temperatures to improve the hydrogen sorption capacity.

4.3.2.1 Energy of sorption for bulk and nanostructured palladium

The energy of sorption value for bulk palladium was determined using the classical Clausius-Clapeyron equation [61] by considering the equilibrium points (plateau region) of the palladium hydride system.

$$\frac{d \ln P}{dT} = \frac{\Delta H}{RT^2} \qquad [17]$$

It is assumed that the energy of sorption does not change with the temperature in equation 17. $\ln P$ vs $\frac{1}{T}$ graph is constructed to determine the energy of sorption value from the slope of the straight line by making use of the equilibrium pressure versus hydrogen composition data at two different temperatures (Figure 46).

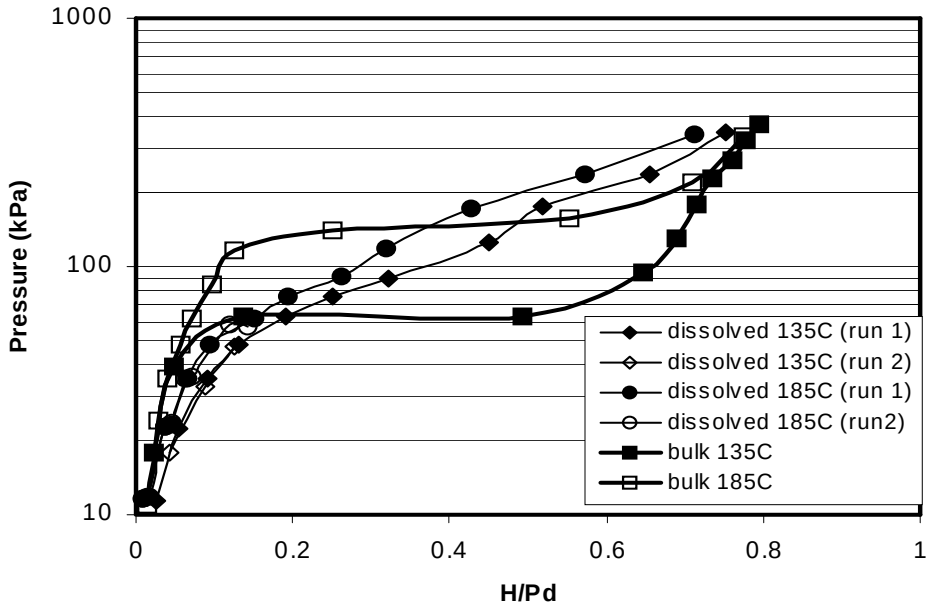

Figure 46. P-C isotherms of dissolved Pd nanowires and bulk Pd at two different temperatures

In our study, we have determined the energy of sorption value from the plateau of the metal hydride isotherm for bulk palladium approximately as 28 kj/mol using two different temperatures. This value is within the range of the previously reported results in different studies [20, 62-64].

Furthermore, it has been shown that energy of sorption was greatly reduced when using Pd nanowires as compared to bulk Pd. It is of great interest to reduce the energy of sorption because of the economical point of view where reducing the energy of sorption will in turn reduce the release temperature and it is the key factor to increase the energy efficiency of the whole system. Energy of sorption values were calculated for the whole

composition range for both bulk Pd and Pd nanowires. In Figure 47, it is seen that nanowires yield a lower energy of sorption value of approximately 7 kj/mol at the plateau pressures.

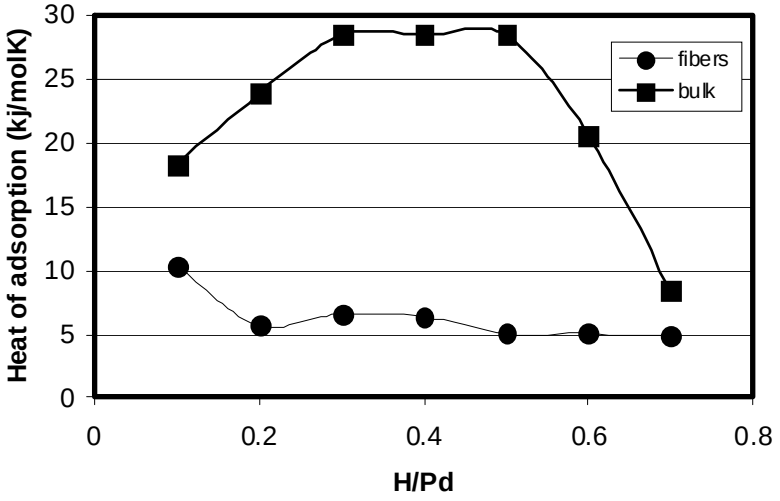

Figure 47. Energy of sorption values corresponding to different H/Pd compositions for fibers (nanowires) and bulk Pd

Since energy of sorption corresponds to the bond strength between hydrogen and palladium, these results indicate that decreasing size of the particles weakens the bond strength between them and lowers the release temperature of the hydrogen by using the nanostructured materials.

As a result of the volumetric experiments, the effect of nanostructuring behavior on the hydrogen sorption capacity of these unique materials having about 100-200 nm particle size produced through template-assisted electrochemical deposition process has

been examined. The results that we have obtained revealed the sorption capacity of the materials having uniform and homogeneous particle size.

The materials at this particle size range clearly show better sorption uptake capacity in the α-phase region. In order to increase the sorption capacity of these materials also in the β-phase, alloys using palladium and some other metals (such as magnesium) with a higher hydrogen uptake capacity can be prepared.

In order to commercialize metal hydrides and use them as efficient hydrogen storage media, other important properties of these unique systems need to be optimized other than storage capacity such as kinetics, cyclability, cost, etc.

CHAPTER V

CONCLUSIONS AND FUTURE WORK

Metal hydrides are considered to be good candidates for hydrogen storage due to their high volumetric and gravimetric hydrogen densities and safe operating conditions. In this study, the major focus was to determine the effect of nanostructuring on the hydrogen uptake behavior of palladium nanowires fabricated using commercial anodized alumina membrane.

Electrodeposition experiments were started with nickel as the test metal and nanostructured nickel was produced in various porous membranes. The effects of deposition time, pore size, porosity, current density and aspect ratio on the fabrication of nickel nanostructures were examined. Nickel nanotubes were obtained with 1,000 nm pore size polycarbonate membranes without any chemical treatment of pore walls. As the deposition time increases, nanotubes turn into solid rods. As the porosity of the membrane increases, the effective current density decreases due to the larger exposed area. Lower porosity and hence higher current density favors the production of hollow nanostructures as was shown by 1,000 nm polycarbonate membranes. However, hollow fibers could not be obtained with smaller size polycarbonate membranes and with

anodized alumina templates even at high current density. We think that below a critical pore size, solid rods are formed through layer by layer mechanism regardless of current density due to the smaller surface area of the pore bottom compared to pore walls. One last parameter that is considered was the aspect ratio. Nanowires were obtained with aspect ratios of 60 and higher while nanotubes were formed at a much lower aspect ratio which is 11. Thus, it is concluded that the morphology of nanostructures is a result of an intricate play between current density, pore size and aspect ratio.

The conditions were also optimized to obtain palladium nanowires using commercial anodized alumina membranes. Palladium nanowires could be obtained when 2 mM electrolyte concentration with an applied potential of 0.5 V used in the experiments. The palladium nanowires could also be obtained by conducting galvanostatic experiments.

The P-C isotherms of the palladium nanowires revealed the major hydrogen uptake behavior of the nanostructured palladium. Enhanced hydrogen capacity at low pressure range, a reduced capacity at higher pressures, a positive slope in the miscibility region and narrowing of the plateau region were observed. The hydrogen uptake capacity of the nanostructured palladium hydride system at 135 ^{o}C up to 100 kPa was found as 0.7 wt%.

The energy of sorption for the bulk palladium was determined from the plateau pressure approximately as 28 kj/mol. Furthermore, it has been shown that energy of sorption was reduced to about 7 kj/mol with nanostructured Pd nanowires. It is of great interest to reduce the energy of sorption because of the economical point of view where

reducing the energy of sorption will in turn reduce the release temperature and it is the key factor to increase the energy efficiency of the system.

In order to commercialize metal hydrides and use them as efficient hydrogen storage media, other important properties of these unique systems need to be optimized other than storage capacity such as kinetics, cyclability, cost etc. Therefore, more fundamental research needs to continue to improve the key factors of metal hydride systems.

BIBLIOGRAPHY

[1] Berube V, Radtke G, Dresselhaus M, Chen G Size effects on the hydrogen storage properties of nanostructured metal hydrides: A review. *International Journal of Energy Research* 2007; 31: 637-663

[2] Sakintuna B, Darkrim FL, Hirscher M Metal hydride materials for solid hydrogen storage. *International Journal of Hydrogen Energy* 2007:32: 1121-1140

[3] Ross DK Hydrogen storage: The major technological barrier to the development of hydrogen fuel cell cars. *Vacuum* 2006; 80: 1084-1089

[4] Fakioglu E, Yurum Y, Veziroglu TN A review of hydrogen storage systems based on boron and its compounds. *International Journal of Hydrogen Energy* 2004; 29: 1371-1376

[5] Dillon AC, Heben MJ Hydrogen storage using carbon adsorbents: past, present and future. *Applied Physics* 2001;A72: 133-142

[6] David E An overview of advanced materials for hydrogen storage *Journal of Materials Processing Technology* 2005; 162-163: 169-177

[7] Chambers A, Park C, Baker RTK, Rodriguez NM Hydrogen storage in graphite nanofibers *The Journal of Physical Chemistry B* 1998; 102: 4253-4256

[8] Rather S, Zacharia R, Hwang SW, Naik M, Nahm KS Hyperstoichiometric hydrogen storage in monodispersed palladium nanoparticles *Chemical Physics Letters* 2007; 438: 78-84

[9] Dornheim M, Eigen N, Barkhordarian G, Klassen T, Bormann R Tailoring hydrogen storage materials towards application *Advanced Engineering Materials* 2006; 8: 377-385

[10] Kishore S, Nelson JA, Adair JH, Eklund PC Hydrogen storage in spherical and platelet palladium particles *Journal of Alloys and Compounds* 2005; 389: 234-242

[11] Tessier P, Akiba E Catalysed reactive milling *Journal of Alloys and Compounds* 1999; 293-295: 400-402

[12] Tessier P, Akiba E Decomposition of nickel-doped magnesium hydride prepared by reactive mechanical alloying *Journal of Alloys and Compounds* 2000; 302: 215-217

[13] Satyapal S, Petrovic J, Read C, Thomas G, Ordaz G The U.S. department of energy's national hydrogen storage project: progress towards meeting hydrogen-powered vehicle requirements *Catalysis Today* 2007; 120: 246-256

[14] Sherif SA, Barbir F, Veziroglu TN Wind energy and the hydrogen economy-review of the technology *Solar Energy* 2005; 78: 647-660

[15] Kohli DK, Khardekar RK, Singh R, Gupta PK Glass micro-container based hydrogen storage scheme *International Journal of Hydrogen Energy* 2008; 33: 417-422

[16] Vajo JJ, Olson GL Hydrogen storage in destabilized chemical systems *Scripta Materialia* 2007; 56: 829-834

[17] Martin M, Gommel C, Borkhart C, Fromm E Absorption and desorption kinetics of hydrogen storage alloys *Journal of Alloys and Compounds* 1996; 238 : 193-201

[18] Reilly JJ, Adzic GD, Johnson JR, Vogt T, Mukarjee S, McBreen The correlation between composition and electrochemical properties of metal hydride electrodes *J Journal of Alloys and Compounds* 1999; 293-295: 569-582

[19] Sastri MVC Introduction to metal hydrides: Basic chemistry and thermodynamics of their formation Berlin, New York: Narosa publishing house (1998)

[20] Jewell LL, Davis BH Review of absorption and adsorption in the hydrogen-palladium system *Applied Catalysis A: General* 2006; 310: 1-15

[21] Yamauchi M, Ikeda R, Kitagawa H, Takata M Nanosize effects on hydrogen storage in palladium *Journal of Physical Chemistry C* 2008; 112: 3294-3299

[22] Pundt A, Suleiman M, Bahtz C, Reetz MT, Kirchheim R, Jisravi NM Hydrogen and Pd-clusters *Materials Science and Engineering* 2004; B108: 19-23

[23] Kay BD, Peden CHF, Goodman DW Kinetics of hydrogen absorption by Pd(110) *Physical Review B* 1986; 34: 817-822

[24] Sachs C, Pundt A, Kircheim R Solubility of hydrogen in single-sized palladium clusters *Physical Review B* 2001; 64:075408-1

[25] Mitsui T, Rose MK, Fomin E, Ogletree DF, Salmeron M Hydrogen absorption and diffusion on Pd(111) *Surface Science* 2003; 540 : 5-11

[26] Pundt A, Kircheim R Hydrogen in metals: microstructural aspects *Annu. Rev. Mater. Res.* 2006; 36: 555-608

[27] Cao G, Liu D Template-based synthesis of nanorod, nanowire, and nanotube arrays *Advances in Colloid and Interface Science* 2008; 136: 45-64

[28] Xue S, Cao C, Zhu H Electrochemically and template-synthesized nickel nanorod arrays and nanotubes *J Mater Sci* 2006; 41: 5598-5601

[29] Pirota KR, Navas D, Velez MH, Nielsch K, Vazquez M Novel magnetic materials prepared by electrodeposition techniques: arrays of nanowires and multi-layered microwires *Journal of Alloys and Compounds* 2004; 369: 18-26

[30] Bao J, Tie C, Xu Z, Zhou Q, Shen D, Ma Q Template synthesis of an array of nickel nanotubes and its magnetic behavior *Advanced Materials* 2006; 13: 1631-1633

[31] Cao H, Xu Z, Hong J, Liu H, Yin G, Li B, Tie C Template synthesis and magnetic behavior of an array of cobalt nanowires encapsulated in polyaniline nanotubules *Advanced Materials* 2001;13: 121-123

[32] Kaur R, Verma NK, Kumar S Fabrication of copper microcylinders in polycarbonate membranes and their characterization *J Mater Sci*, 2006; 41: 3723-3728

[33] Xiao J, Xie Y, Tang R, Chen M, Tian X Novel ultrasonically assisted templated synthesis of palladium and silver dendritic nanostructures *Advanced Materials* 2001; 13: 1887-1891

[34] Wang Q, Wang G, Xu B, Jie J, Han X, Li G, Li Q, Hou JG Non-aqueous cathodic electrodeposition of large-scale uniform ZnO nanowire arrays embedded in anodic alumina membrane *Materials Letters* 2005; 59: 1378-1382

[35] Chan LH, Hong KH, Lai SH, Liu XW, Shih HC The formation and characterization of palladium nanowires in growing carbon nanotubes using microwave plasma-enhanced *Thin Solid Films* 2003;423: 27-32

[36] Zhang M, Lenhert S, Wang M, Chi L, Lu H, Ming N Regular arrays of copper wires formed by template-assisted electrodeposition *Advanced Materials* 2004; 16: 409-412

[37] Nielsch K, Muller F, Li AP, Gosele U Uniform nickel deposition into ordered alumina pores by pulsed electrodeposition *Advanced Materials* 2000; 12: 582-586

[38] Lee BK, Lee SM, Cheon J Size-controlled synthesis of Pd nanowires using a mesoporous silica template via chemical vapor infiltration *Advanced Materials* 2001; 13: 517-520

[39] Schwarzacher W, Kasyutich OI, Evans PR, Darbyshire MG, Yi G, Fedosyuk VM, Rousseaux F, Cambril E, Decanini D Metal nanostructures prepared by template electrodeposition *Journal of Magnetism and Magnetic Materials* 1999; 198-199: 185-190

[40] Naohara H, Ye S, Uosaki K Electrochemical deposition of palladium on an Au(111) electrode: effects of adsorbed hydrogen for a growth mode *Colloids and Surfaces A* 1999; 154: 201-208

[41] Jagminas A, Kurtinaitiene M, Angelucci R, Valincius G Modification of alumina barrier-layer through re-anodization in an oxalic acid solution with fluoride additives *Applied Surface Science* 2006 ; 252: 2360-2367

[42] Kim KT, Cho SM A simple method for formation of metal nanowires on flexible polymer film *Materials Letters* 2006; 60: 352-355

[43] Motoyama M, Fukunaka Y, Sakka T, Ogata YH, Kikuchi S Electrochemical processing of Cu and Ni nanowire arrays *Journal of electroanalytical chemistry* 2005; 584: 84-91

[44] Kerman K, Saito M, Yamamura S, Takamura Y, Tamiya E Nanomaterial-based electrochemical biosensors for medical applications *Trends in Analytical Chemistry* 2008; 27: 585-592

[45] Monch I, Meye A, Leonhardt A, Kramer K, Kozhuharova R, Gemming T, Wirth MP, Buchner B Ferromagnetic filled carbon nanotubes andnanoparticles: synthesis and lipid-mediated delivery into human tumor cells *Journal of Magnetism and Magnetic Materials* 2005; 290: 276-278

[46] Aravamudhan S, Ramgir NS, Bhansali S Electrochemical biosensor for targeted detection in blood using aligned Au nanowires *Sensors and Actuators B* 2007; B127: 29-35

[47] Kim KT, Sim SJ, Cho SM Hydrogen gas sensor using Pd nanowires electro-deposited into anodized alumina template *IEEE SENSORS JOURNAL* 2006; 6: 509-513

[48] Panovic M, Modern Electroplating New York: Wiley; (2000)

[49] Bard, Allen J.; Parsons, Roger; and Jordan, Joseph, Standard Potentials in Aqueous Solutions New York: Marcel Dekker (1985)

[50] Bard, Allen J., and Faulkner, Larry R Electrochemical Methods: Fundamentals and Applications New York: Wiley (2000)

[51] Milazzo G, Caroli S, Sharma VK Tables of Standard Electrode Potentials, Wiley, Chichester (1978)

[52] Bratsch SG Standard electrode-potentials and temperature coefficients in water at 298.15K *J of Physical and chemical reference data* 1989; 18: 1-21

[53] Cao H, Wang L, Qiu Y, Wang G, Zhang L, Liu X Generation and growth mechanism of metal (Fe, Co, Ni) nanotube arrays *CHEMPHYSCHEM* 2006; 7: 1500-1504

[54] Tao F, Guan M., Jiang Y, Zhu J, Xu Z, Xue Z An easy way to construct an ordered array of nickel nanotubes: the triblock-copolymer-assisted hard-template method *Advanced Materials* 2006; 18: 2161-2164

[55] Rahman IZ, Razeeb KM, Kamruzzaman Md, Serantoni M Characterization of electrodeposited nickel nanowires using NCA template *Journal of Materials Processing Technology* 2004; 154: 811-815

[56] Liu Y, Ma D, Blackley RA, Zhou W, Han X, Bao X Synthesis and characterization of Gibbsite nanostructures *J of Phys. Chem. C.* 2008; 112: 4124-4128

[57] Vasconcelos EA, Santos FRP, Silva EF, Boudinov H Nanowire growth on Si wafers by oxygen implantation and annealing *Applied Surface Science* 2006; 252:5572-5574

[58] Broom DP, Moretto P Accuracy in hydrogen sorption experiments *Journal of Alloys and Compounds* 2007; 446: 687-691

[59] Kuji T, Matsumura Y, Uchida H, Aizawa T Hydrogen absorption of nanocrystalline palladium *Journal of Alloys and Compounds* 2002;330-332: 718-722

[60] Yamauchi M, Kitagawa H Hydrogen absorption of the polymer-coated Pd nanoparticle *Synthetic Metals* 2005; 153: 353-356

[61] Smith, J.M., Van Ness H.C., Abbott, M.M., Chemical Engineering thermodynamics, 6th Ed, McGraw-Hill Companies, Inc., 2001]

[62] Bogdanovic B, Brand RA, Marjanovic A Metal doped sodium aluminum hydrides as potential new hydrogen storage materials *Journal of Alloys and Compounds* 2000; 302: 36-58

[63] Krishnankutty N, Vannice MA The effect of pretreatment on Pd/C catalysts I. adsorption and absorption properties *Journal of Catalysis* 1995; 155: 312-326

[64] Tomanek D, Sun Z, Louie SG Abinitio calculation of chemisorption systems – H on Pd (001) and Pd (110) *Physical Review B* 1991; 43: 4699-4713

APPENDIX

A. Helium expansion measurements

The volume of the custom-built system was determined by helium expansion measurements. In these measurements, helium gas was expanded from the unknown volume to known volume or vice versa (Figure A1). We made use of material balances and ideal gas equation of state in the calculations. The equations are shown below. In these equations, "R" denotes the reference side whereas "S" denotes the sample side. During the charging of the gas and in the expansion steps, the pressures and temperatures of both sides before and after gas expansion were measured through pressure and temperature transducers. Therefore, by using these data and the known volume, the unknown volume can be determined easily.

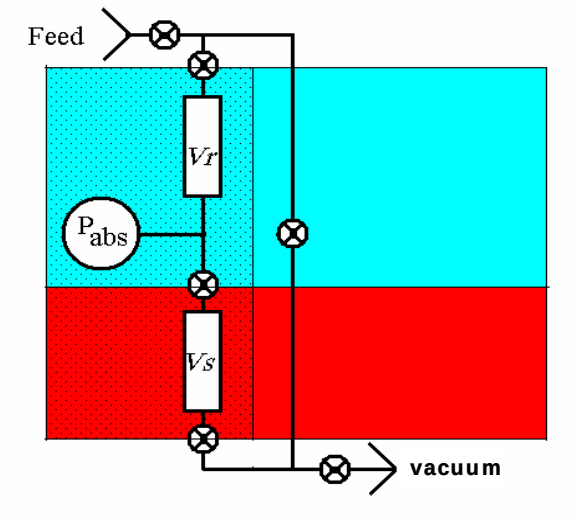

Figure A1. General volumetric system to show the principle of helium expansion measurement

$$\frac{P_{i-1}V_s}{RT_s} + \frac{P_i^{ch}V_R}{RT_R} = \frac{P_i^{\exp}V_s}{RT_s} + \frac{P_i^{\exp}V_R}{RT_R} \tag{18}$$

$$\left(\frac{P_i^{\exp} - P_{i-1}^{col}}{RT_s}\right) V_s = \left(\frac{P_i^{ch} - P_i^{\exp}}{RT_R}\right) V_R \tag{19}$$

$$\frac{V_s}{V_R} = \alpha = \frac{\dfrac{P_i^{ch} - P_i^{\exp}}{T_R}}{\dfrac{P_i^{\exp} - P_{i-1}^{col}}{T_s}} \tag{20}$$

B. Gas sorption measurements

In determination of the amount of gas adsorbed, similarly, material balances and equation of states were used. The principle is the same as in helium expansion measurements. P-V-T data before and after gas expansions are used to determine the amount absorbed at every step by using the below stated material balances.

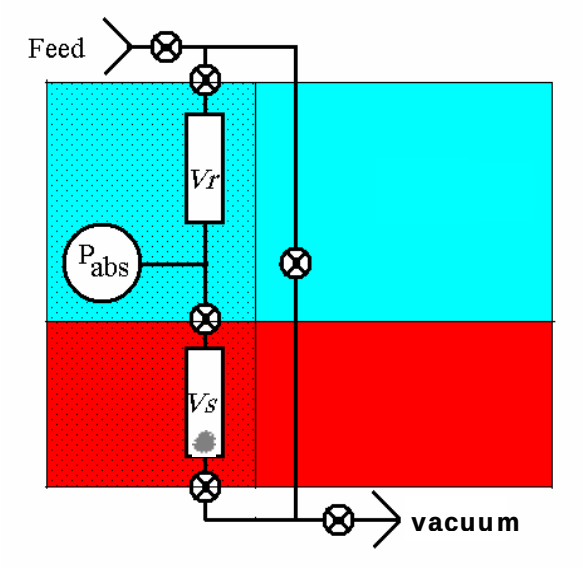

Figure A2. General volumetric system to show the principle of gas sorption measurement when there is sample in the sample cell

$$\frac{P_{i-1}^{col}V_s}{RT_s}+\frac{P_i^{ch}V_R}{RT_R}=\frac{P_i^{\exp}V_s}{RT_s}+\frac{P_i^{\exp}V_R}{RT_R}+m\left(n_i-n_{i-1}\right) \tag{21}$$

$$m\left(n_i-n_{i-1}\right)=V_s\left(\frac{P_{i-1}^{col}-P_i^{\exp}}{RT_s}\right)+V_R\left(\frac{P_i^{ch}-P_i^{\exp}}{RT_R}\right) \tag{22}$$

$$\frac{Rm\left(n_i-n_{i-1}\right)}{V_R}=\frac{P_i^{ch}-P_i^{\exp}}{T_R}+\alpha\left(\frac{P_{i-1}^{col}-P_i^{\exp}}{T_s}\right) \tag{23}$$